Enhancing Coastal Flood Resiliency in Canada through Hazard and Life Safety Assessments

Joseph Kim

A thesis submitted to the University of Ottawa in partial fulfillment of the requirements for the

Master of Applied Science in Civil Engineering

Academic advisor: Prof. Ioan Nistor

uOttawa

Faculty of Engineering
University of Ottawa

Abstract

Home to the world's longest coastline, Canada has experienced devastating economic and social from coastal flooding events. While there have been a variety of mitigation methods employed over the years to increase a community's resistance to coastal hazards, it is unrealistic to think that there exists a solution to guarantee a community's safety under all possible flood hazards. Instead, the community's efforts to raise their resistance to flood hazards should be augmented with careful planning and management to increase a community's resilience to flood hazards, allowing them to recover quickly after a natural disaster. The first step in elevating a community's resilience is to better understand the expected hazards that it may experience.

This thesis presents two unique case studies to better understand the flooding hazards present on the Canadian coastline. A large-scale numerical model that accounts for the presence of ice was developed to investigate storm surges in Canada's western Arctic. It was found that the quality of the climatic forcing data used, ERA5, was poor in capturing peak wind speeds, but could be compensated for by using elevated wind drag coefficients. The use of non-traditional high-water marks such as driftwood lines were validated and were shown to significantly alter expected flood return periods compared to the return periods estimated from only the incomplete tide gauge measurements present on the Arctic coastline.

The second case study extends the results of a tsunami hydrodynamic simulation on Canada's Pacific coastline through a life safety assessment. The performance between an agent-based and GIS-based approach to modelling tsunami evacuation were directly compared and were shown to yield different magnitudes in fatality rate and facility demand, but similar trends. Both models agreed on a mitigation option that can significantly reduce the loss of life during a tsunami.

Acknowledgements

First and foremost, I would like to express my utmost gratitude to my academic supervisor, Prof. Ioan Nistor. Ever since my interest in coastal engineering was sparked during my undergraduate studies, he has always provided me with countless opportunities and resources to pursue research that I find personally interesting. In addition to his timely and valuable technical expertise which has led to the improvement of all the works I produce, I especially value the patience and trust he exhibits towards his students. Needless to say, this thesis would not have been possible without his dedication.

During my research visit at Waseda University, Tokyo, Japan, I was warmly welcomed by all the members of the Shibayama Lab. Prof. Shibayama was always happy to share his vast knowledge of coastal engineering despite his busy schedule. My sincere appreciation goes to Dr. Takabatake who has taught me everything I know about performing life safety assessments and has been a constant source of critical feedback. Ms. Emiko Matsumaru also dealt with all the logistics involved with relocating from Ottawa to Tokyo for the research visit. I would also like to thank all the lab members of Shibayama lab for their warm hospitality and interesting discussions during my stay there.

I am also grateful towards my colleagues at the Ocean, Coastal, and River Engineering Research Centre at National Research Council Canada. My close collaborators, Mr. Enda Murphy, Mr. Sean Ferguson, and Mr. Mitchel Provan provided me with training from their years of accrued technical expertise as I learned to perform hazard assessments from the ground up. Additionally, all the members of the Ice and Water Resources team and external project collaborators were sources of discourse and fresh insight throughout my work.

Lastly, this work would have not been possible without the eternal support of my family and friends. To my parents, thank you for your unconditional support in whatever I choose to do. To my friends, thank you for your moral support during the difficult times.

Table of Contents

List of Figures

List of Tables

List of Acronyms

ABM	Agent-Based Modelling
ASCE	American Society of Civil Engineers
BC	British Columbia
CD	Chart Datum
CFL	Courant-Friedrich-Lewy
CHS	Canadian Hydrographic Service
CIS	Canadian Ice Service
CMCLP	Capacitated Maximal Covering Location Problem
CSZ	Cascadia Subduction Zone
D/C	Demand-Capacity
DV	Depth-Velocity
ECCC	Environment and Climate Change Canada
ERA5	European Centre for Medium Range Weather Forecasts Re-Analysis 5
GEBCO	General Bathymetric Chart of the Oceans
GIS	Geographical Information System
GPD	Generalized Pareto Distribution
MCLP	Maximal Covering Location Problem
MSL	Mean Sea Level
Mw	Moment Magnitude
NSIDC	National Snow and Ice Data Centre
OD	Origin Destination
PST	Pacific Standard Time
RMSE	Root-Mean-Squared-Error
SD	Summer Daytime
SN	Summer Night-time
WAFO	Wave Analysis and Fatigue and Oceanography

List of Symbols

$AF = the\ area\ fraction\ of\ ice\ coverage$

$C_d = wind\ drag\ coefficient$

$C_{d-w} = air - sea\ drag\ coefficient$

$C_{d-is} =\ ice\ skin\ drag$

$\lambda = longitude\ (°)$

$\varphi = latitude\ (°)$

$z = normal\ vertical\ distance\ from\ the\ initial\ water\ surface\ (m)$

$\eta = water\ surface\ elevation\ (m)$

$D = total\ water\ depth\ (m)$

$M = discharge\ flux\ in\ the\ \lambda\ direction\ (\frac{m^3}{s})$

$N = discharge\ flux\ in\ the\ \phi\ direction\ (\frac{m^3}{s})$

$n = Manning's\ roughness\ coefficient\ (\frac{s}{m^{\frac{1}{3}}})$

$g = gravitational\ acceleration\ (m^2/s)$

$R = radius\ of\ the\ Earth\ (m)$

$f = 2\omega sin\phi = Coriolis\ parameter$

$\omega = angular\ velocity\ of\ the\ Earth's\ rotation\ (s^{-1})$

$\rho = crowd\ density = \left(\frac{the\ number\ of\ agents\ on\ a\ road}{the\ area\ of\ a\ road\ (m^2)}\right)$

$v_{walking} = walking\ speed\ (\frac{m}{s})\ as\ defined\ by\ Knoblauch\ et\ al.\ (1996)$

$d_{evacuee} = distance\ that\ the\ evacuee\ can\ travel\ \ (m)$

$v_{evacuee} = velocity\ of\ the\ evacuee\ (\frac{m}{s})$

$t_{available} = time\ available\ for\ evacuation\ (s)$

Chapter 1 Introduction

1.1 Motivation

Humankind has been obsessed with the destructive properties of water since the beginning of time—so much so that they have been the prime focus of countless biblical, mythological, and cultural stories. Many of these fables, such as in the story of Noah's Ark, floods signified the "reversal of creation", yet we (as in humankind) are still drawn to the allure of water. We pay premiums on our properties to have a waterfront, vacation in coastal areas, and take part in leisure activities out by the ocean. Perhaps, this is due to the fact that there have been countless studies showing the benefits to your psychological and physical well-being by being near an open body of water (Borja et al., 2020; Völker and Kistemann, 2013; White et al., 2013). However, the crux of this matter is that while it is not to the extent of a "reversal of creation" as told in those aforementioned historical stories, floods have plagued our communities and have resulted in large-scale social and economic losses across the globe (Kundzewicz et al., 2014). To combat these dangers, engineers and emergency managers have studied and invested in mitigation and adaptation measures, however it is unlikely that any interventions can fully guarantee a community safe from floods. Thus, a community's ability to resist disasters should be compounded by the planning and construction of resilient infrastructure to accelerate the recovery process (Shrubsole, 2013). This begs the question— how do we plan for more flood resilient communities?

1.2 Research Objectives

Jonientz-Trisler (2004) summarized the framework for planning tsunami resilient communities (although this concept can generalised to planning resilient communities to other coastal flood hazards) by Dengler (1998) as three components: hazard assessment, warning guidance and mitigation. This thesis aims to increase coastal resiliency on Canada's shoreline by performing evidence-based case studies to improve on the knowledge of the first component (hazard assessment) by:

(1) Advancing the knowledge of storm surge hazard modelling through a case study where the unique aspects of ice presence and limited data availability are accounted for.

(2) Extending the results of hydrodynamic hazard modelling by providing more value-added products such as life safety assessments to coastal communities.

1.3 Scope of Work

While flooding can present itself through a wide array of pathways, this thesis focuses on coastal hazards. In particular, the hazards associated with earthquake-generated tsunamis and storm surges due to forcing from atmospheric weather systems are investigated. Recent advancements in climatic reanalysis datasets and cold-regions science present an opportunity to investigate storm surge phenomena with greater technical and computational rigour. To address the first objective a numerical investigation to better understand the storm surge hazard in Canada's western Arctic was conducted. The utility of the European Centre for Medium Range Weather Forecasts Re-Analysis 5 (ERA5) to force numerical simulation of storm surge was explored. Storm surge events that were captured on the tide gauge near Tuktoyaktuk were identified and simulated while accounting for the impacts of sea ice storm surge elevations. Due to the lack of gauge measurements in the Arctic, the numerical model was also used to hindcast an event that was not captured by the tide gauge record, but

where high-water elevations could be otherwise approximated from observed driftwood lines.

Soft measures such as evacuation planning are recommended to mitigate the loss-of-life during tsunamis. Two types of numerical models are widely used to assess a community's evacuation potential. Agent-based modelling (ABM) defines sets of rules that each agent in the simulation must follow during the simulated evacuation. By doing this, the dynamic and complex interactions between the agents and the environment can be accounted for but requires substantial specialized knowledge to implement. Geographical information systems (GIS) are much more common and widely used by city planners and emergency coordinators. While GIS has also been used to simulate evacuations, it lacks the ability to incorporate the dynamic behaviours that ABMs can account for. To address the second objective, the two evacuation modelling methodologies were directly compared through a case study for Tofino, BC, Canada by assessing the state of evacuation preparedness and investigating potential mitigation options.

1.4 Novelty of Study

This thesis presents two separate case studies with their own unique novelties. The first case study is the first large-scale numerical study investigating storm surges in Canada's western Arctic since Danard et al. (1989). Since that time, computational power has increased exponentially, allowing for the use of large domains with high resolution unstructured grids to capture the development of storm surges due to momentum transfer between air and sea. Additionally, studies at that time used surface winds calculated from geostrophic winds (which were obtained from pressure fields). With the recent issuance of high-resolution datasets such as ERA5, climate reanalysis datasets can now be used as climatic forcing input in storm surge models. However, a thorough investigation on the quality of ERA5 has not been assessed due to its recent release. This study offers the first analysis on the reliability of ERA5 during stormy

periods in the Canadian Arctic and offers a solution to overcome some of its deficiencies. The first case study also attempts to validate the use of non-traditional sources such as driftwood lines as high-water marks. This is particularly important as long-standing and complete tide gauge records in the Arctic are rare.

The second case study is among the first to apply an ABM to simulate tsunami evacuation in Canada. While ABMs are thought to be superior when modelling evacuation scenarios due to their ability to incorporate time-based behaviours (Mas et al., 2015), commercial GIS products provide simple user interfaces to model location-allocation problems (which can be used for evacuation planning). Additionally, many emergency planners and engineers are familiar with GIS, which foregoes the requirement to have specialized knowledge to set-up an ABM to assess the evacuation potential of their community. The actual differences between the performances of the two evacuation modelling strategies have never been directly compared until this study.

1.5 Outline of the Thesis

Chapter 1 serves as a preface to the thesis by providing: background information on the motivation of the study, the objective, scope of work, and the novelty of the works presented in this thesis.

Chapter 2 presents an overview on the history and current state of flood management guidance in Canada and identifies research needs to plan for more resilient communities.

Chapter 3 presents a technical paper that investigates storm surges in Canada's western Arctic through a numerical storm surge model that accounts for the presence of ice. In the process, the quality of the ERA5 dataset and the tide gauge records in the western Arctic of Canada are analyzed. The validity of using non-traditional in lieu of tide gauge records was also investigated. This work was performed at National Research Council Canada under the Canadian Safety and Security Program, administered by Defense

Research and Development Canada. The author performed the numerical modelling and analysis of the experiment under the guidance of Mr. Enda Murphy, Mr. Sean Ferguson, Mr. Mitchel Provan, and Dr. Ioan Nistor.

Chapter 4 presents a technical paper that directly compares the performance of two evacuation modelling frameworks: GIS and ABM. During this process, the effects of crowd density are incorporated into an ABM, and mitigation options to minimize the loss of life for the study's community are investigated and identified. This work was performed at Waseda University in collaboration with the District of Tofino, BC, Canada. The author designed the experiment and performed the analysis. The numerical modelling was performed by the author and Dr. Tomoyuki Takabatake. This work was performed under the guidance of Dr. Tomoyuki Takabatake and Dr. Ioan Nistor.

Chapter 5 presents the conclusions of the thesis and provides suggestions for future studies.

Chapter 2 An Overview on the State of Canadian Flood Hazard Management Practices

2.1 On the Concept of Resiliency

Urbanisation in Canada has historically been focused near the coastline and other large bodies of water. Manson (2005) estimated that in 2001, 38.3% of the Canadian population lived within 20km of a coast (i.e. the Atlantic, Arctic, Pacific and Great Lakes coasts), which only accounts for 2.6% of Canada's total area. This trend of people wanting to reside by open bodies of water will likely not change in the near future as the majority of coastal communities are expected to see increases in population (Manson, 2005). To counteract the increasing vulnerability to coastal communities, planning for a resilient response to natural disasters have been recommended as an effective flood management strategy (Moudrak and Feltmate, 2019).

The term "resiliency" was first coined by Holling (1973) when he used it to describe ecological systems:

> *"Resilience determines the persistence of relationships within a system and is a measure of the ability of these systems to absorb changes of state variables, driving variables, and parameters, and still persist."*

This definition persists to this day and has seen widespread adoption among practitioners of coastal management. Resilience allows a system (i.e in the context of this thesis, a community) to absorb a change of parameters (i.e a flood hazard) while remaining within an acceptable state. This can lead the system to quickly adapt and learn from the sudden change of parameters, allowing potential development and learn lessons during the renewal process to better deal with future disturbances to the system (Folke et al., 2002). While the definition seems straightforward and easy to understand,

planning for resilient coastal communities presents a difficult challenge that requires the expertise and input from multiple parties. After the devastation from the Indian Ocean tsunami of December 2004, the U.S. Indian Ocean Tsunami Warning System Program (2007) issued a report detailing important elements that a resilient community should demonstrate:

- Governance: The leadership and legal framework provided by the government to aid communities to build resilience.

- Society and Economy: The engagement with sustainable and diverse livelihoods that can withstand coastal hazards.

- Coastal Resource Management: Active conservation and management of coastal resources to reduce risk from coastal hazards.

- Land Use and Structural Design: Land use policies and structural intervention to protect the economic, environmental and social infrastructure.

- Risk Knowledge: An acute awareness of the potential hazards and risks that the community face among leaders and community members.

- Warning and Evacuation: In the event of a natural disaster, the dissemination of warnings to community members and at-risk populations, for appropriate response during an evacuation.

- Emergency Response: An established system for a community to quickly respond to and address the emergency needs due to a coastal disaster.

- Disaster Recovery: A prepared plan prior to hazard events to effectively resist environmental, social and economic impacts cause by the hazard event, and coordinate the recovery process.

In the pursuit of the development of these characteristics of flood resiliency, a number of guidelines and frameworks have been issued by varying levels of government over the years.

2.2 State of Flood Management Practices in Canada

A timeline of major milestones and initiatives enacted by the Federal Government of Canada related to flood management policies and studies can be seen in Figure 1.

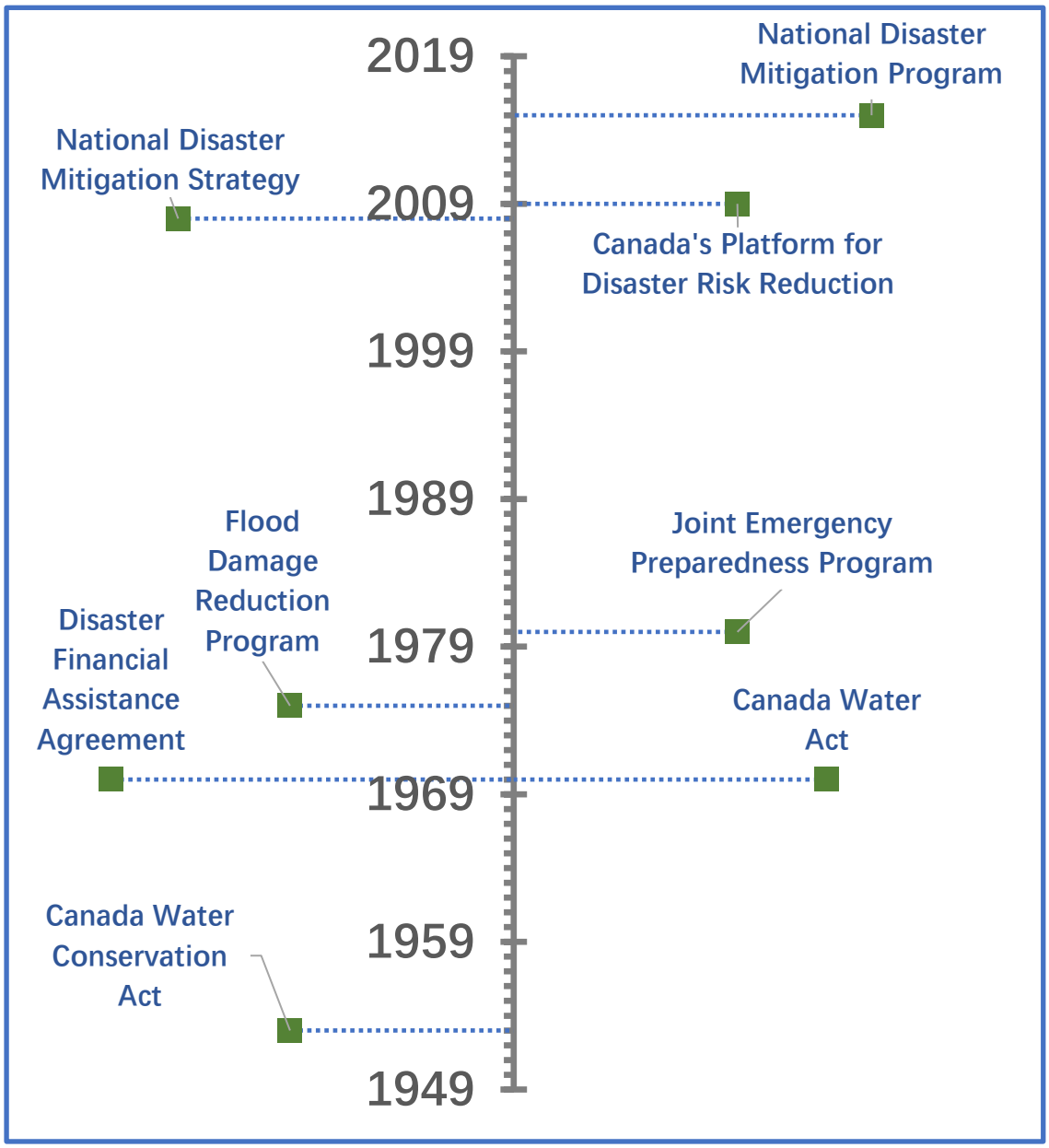

Figure 1: Overview of major flood management initiatives directed by the Federal Government of Canada

The *Canada Water Conservation Assistance Act* of 1953 was the first piece of federal legislation that dealt directly with water resource management. This legislation was introduced to provide funding from the federal government to provincial water storage and flood control projects. However, only a small number of flood control projects were funded under this *Act*. The *Canada Water Conservation Assistance Act* drew critique for its rigid requirements that placed a heavy emphasis on structural mitigation options (Quinn, 1985). The structural mitigation options preferred by the *Canada Water Conservation Act* led to increased urban and agricultural development near hydraulic structures and rivers as there was a perception that floods could be safely controlled, inevitably leading to increased flood damages (Shrubsole, 2013). The *Canada Water Conservation Assistance Act* was also scrutinized for the lack of support and input from the federal government on the planning of flood mitigation projects outside of financial matters (Booth and Quinn, 1995).

The critiques of the flood management methodologies in the *Canada Water Conservation Assistance Act* led to its eventual repeal (Booth and Quinn, 1995) and was replaced with the *Canada Water Act* of 1970. Under the *Canada Water Act*, the *Flood Damage Reduction Program* was introduced to better coordinate the federal and provincial strategies for flood management and oversaw the introduction of non-structural approaches to flood management strategies. Under the *Federal Damage Reduction Program*, the roles between the federal and provincial governments were reversed—the federal government took leadership by pioneering a national program focused on flood risk mapping. This sudden change in accountability may have been due to several large flood events that occurred in 1973 and 1974, allowing for provincial officials to cite these events when persuading federal officials to be more involved in the flood management process (Thomson, 1984; Watt, 1995). While there was some controversy over the limited work performed on Aboriginal lands and on the consistency of the works performed, this program was extremely successful at

redirecting development from flood prone areas (Watt, 1995). By 1975, the development of floodplain mapping was well underway and during the period 1975 and 1996, 28,000 kms of rivers and streams were mapped (MMM Group Limited, 2014). However, mapping of coastal areas and the characterization of coastal hazards was limited. Two additional initiatives, the *Disaster Financial Assistance Agreement* and the *Joint Emergency Preparedness Program*, were developed soon along with the introduction of the *Canada Water Act*. These two programs introduced the core concepts of flood resiliency in federal flood management strategies by focusing on financial aid to accelerate recovery after a disaster, and investing in emergency planning and response respectively.

By the early 2000s, Environment Canada, the federal agency that led the *Flood Damage Reduction Program*, withdrew from the program and flood mapping ceased. Shrubsole (2013) labels the span of 1998 to 2006 as a period of "paralysis and … non-development of a national policy/strategy". This is in part due to three major natural disasters that occurred in the late 90's: the Saguenay River Flood in 1996, the Red River Flood in 1997, and the Eastern Canada Ice Storm in 1998. These three events cost the Canadian government approximately 366 million dollars—by comparison, no single event required more than 30 million dollars in disaster assistance funds prior to 1996 (Hwacha, 2005). These three events forced the federal government to reconsider its national disaster management plan and spurred discussions dating to 1998 which eventually led to the creation of the *National Disaster Mitigation Strategy* in 2008 (Shrubsole, 2013). The idea of resilience was cemented into Canada's flood management strategies through the *National Disaster Mitigation Strategy*'s primary goal (Public Safety Canada, 2008):

> *"To protect lives and maintain **resilient**, sustainable communities by fostering disaster risk reduction as a way of life."*

However, while the principles noted in in the *National Disaster Mitigation Strategy*

were in the right direction, no action to further develop, implement or finance the new paradigm were taken until 2006 (Shrubsole, 2013). By 2006, some of the leadership seen by the federal government during the *Flood Damage Reduction Program* was passed back to the provincial and municipal governments (Richardson et al., 2010). Richardson et al. (2010) also demonstrated a framework for integrating climate change impacts by performing case studies across the nation.

In recent years, *Canada's Platform for Disaster Risk Reduction* was established to coordinate discussions on priorities in disaster risk reduction (such as the Sendai Framework for Disaster Risk Reduction (United Nations Office for Disaster Risk Reduction, 2015) that the group endorsed) through connecting more than 700 members among multiple organizations (Public Safety Canada, 2018a). In 2015, a five-year *National Disaster Mitigation Program* was introduced to address the directions noted in the *National Disaster Mitigation Strategy*. Under the *National Disaster Mitigation Program*, the *Federal Flood Mapping Guideline Series* (Public Safety Canada, 2018b) was produced, offering a framework and technical guidance in performing flood hazard delineation studies.

2.3 Discussion

Over the years, Canada has been heading towards the direction of planning for more flood resilient communities, yet while the policies enacted are to address overall flood hazard in Canada, guidance in dealing with coastal flooding hazards is severely lacking. The *Federal Flood Mapping Guideline Series* (Public Safety Canada, 2018b) issued a document in 2019 with high-level technical advice on performing flood hazard delineations in coastal areas. However, there is tremendous variability between our Pacific, Atlantic, and Arctic coastlines (Lemmen et al., 2016) and generalized procedures may not necessarily fully capture the unique challenges in assessing flood hazard in these areas. While the increased attention to riverine flooding may be due to the fact that it has historically caused more economic damage compared to coastal

flooding (Government of Canada, 2018), Canada's shorelines are experiencing increasing exposure and vulnerability to flooding. The accelerated urbanisation along shorelines (Manson, 2005), increasing levels of flooding from storm surges due to the impacts of climate change (Webster et al., 2006), and the potential for economic losses in the tens of billions of dollars from a Cascadia Subduction Zone earthquake and tsunami (Clague, 2002) demonstrate the need for further advancement in coastal hazard guidelines at the federal level.

While studies performed by the provincial governments can provide insight on the localized challenges in dealing with flood hazards in the area, federal guidelines are especially important in setting a national standard that hazard assessments should strive for. This is critical for the domain of coastal/hydraulic engineering where no codes exist (unlike in structural and geotechnical engineering) that provide the minimum standards for works produced. A federal initiative would also provide the resources to investigate important, but under-studied areas such as Canada's north coast.

2.4 Link to Chapter 3

An overview on the evolution of flood management practices in Canada was presented in Chapter 2. The *Bibliography of Best Practices and References for Flood Mitigation* produced for the *Federal Flood Mapping Guidelines Series* (Public Safety Canada, 2018b) provides a comprehensive list of publications and case studies that demonstrate the best practices related to flood mitigation. In that list, case studies focusing on the coastal hazards that the north coast of Canada experiences are limited and Chapter 3 provides an evidence-based case study to inform future guideline development.

Chapter 3 Technical Paper – Numerical Investigation on Storm Surges in the Beaufort Sea[1,2]

3.1 Introduction

Extreme weather events along Canada's Arctic seaboard produce surges in sea level elevations, which have led to flooding in local communities. During the 1970s and 1980s, a series of studies were initiated by the Beaufort Sea Project focused on assessing the hazard of storm surges in the Arctic. The studies were motivated, in part, by increasing Canadian interest in offshore drilling in the region. These early studies led to the characterization of the weather patterns in the Beaufort Sea, and the development of low-resolution storm surge models forced by surface winds calculated from estimated geostrophic winds (Burns and Service, 1973; Henry, 1975, 1974; Henry and Heaps, 1976). During that time period, validation of storm surge models was not possible due to the lack of recorded storm surge events. Kowalik (1984) simulated three storm surge events in the Beaufort and Chuckchi seas that occurred during ice-free periods using interpolated surface winds from 6-hour calculations of geostrophic winds.

Since that time, high-resolution climatic forcing data have become available in the form of reanalysis datasets. Of particular interest is the newly issued ERA5 reanalysis (Hersbach et al., 2020) which supersedes the older ERA-Interim and promises higher spatial and temporal resolution, and accuracy. While there have been some studies that assess the performance of ERA5 in approximating surface winds and pressures (Graham et al., 2019; Ramon et al., 2019), these studies did not investigate, in detail,

---

[1] Joseph Kim, Enda Murphy, Ioan Nistor, Sean Ferguson, Mitchel Provan "Numerical Investigation on Storm Surges in the Beaufort Sea", In submission process.

[2] A related study, "Numerical Simulation of Storm Surges and Flood Hazards on the Beaufort Sea Coast", Joseph Kim, Sean Ferguson, Mitchel Provan, Enda Murphy, Ioan Nistor, was accepted as an oral presentation for the Coastal Zone Canada 2020 conference. The conference was delayed due to COVID-19.

ERA5's ability to capture sudden changes in weather caused by storminess. Currently, ERA5's suitability to support investigation of extreme weather phenomena, such as storm surge, has not been assessed and reported in existing literature.

In 1977, Reimnitz and Maurer (1979) conducted field investigations along northern Alaska, USA, providing insight to a particularly large storm surge event that occurred on September 13th, 1970. Reimnitz and Maurer (1979) deduced sea-level elevations associated with the 1970 event from a field survey of driftwood debris lines deposited after the storm. Similarly, Harper et al. (1988) surveyed driftwood debris lines in the Tutktoyaktuk, Canada region, located on the shorelines of the Beaufort Sea, and provided estimates of maximum storm surge elevations for the area. Since the field investigations were conducted, more-significant storm surge events have not occurred. In addition, the survey produced detailed storm surge elevation estimates for an event that occurred on August 23rd, 1986.

Accurate simulation of storm surge in Arctic regions can be challenging owing to the presence and dynamics of sea ice, which can dampen the impacts of storm surges (Murty and Polavarapu, 1979). While the numerical model developed by Kowalik (1984) coupled the interaction between ice and water, the performance of their integration was not tested as only ice-free events were simulated during their study. Danard et al., (1989) attempted to refine the inclusion of ice cover by simulating eight cases occurring during the months of August, September, and October. The study showed reasonable success, but computational limits of the era and insufficient spin-up time precluded proper stress transfer between the wind and ocean. Joyce et al., (2019) demonstrated the performance of a new set of formulas that improve on the work of Chapman et al., (2009) to account for the presence of ice for storm surges in western Alaska. All four scenarios that they simulated yielded root-mean-square-errors of less than 20 cm.

In this study, we examine the utility of the ERA5 reanalysis dataset as climatic forcing input for storm surge modelling in Canada's western Arctic region. A two-dimensional hydrodynamic model of the region was developed using TELEMAC-2D software. Customized subroutines were employed to incorporate the impacts of sea ice on storm surge as per Joyce et al., (2019). Model performance was evaluated through the simulation of fifty historical storm surge events which span a range of sea ice conditions ranging from heavy ice cover to open-water conditions. Subsequently, a hindcasting exercise was conducted to compare simulated results to surveyed driftwood lines cited in literature. Roughly 30 years have passed since Harper et al., (1988) provided estimates on the maximum storm surge elevations through a survey on driftwood lines. This paper attempts to validate those experimental results by developing a simulated hindcast of the storm surge event that occurred on August 23rd, 1986. To the knowledge of the authors, there have been no attempts to conduct a large-scale numerical investigation to assess storm surge hazards in the Beaufort Sea since the research conducted by Danard et al., (1989). Since that time, updated and more-refined data sources have become available, and computational power has increased exponentially, permitting lengthier and higher–resolution simulations.

3.2 Methodology

An overview of the study's methodology for reference can be seen in Figure 2.

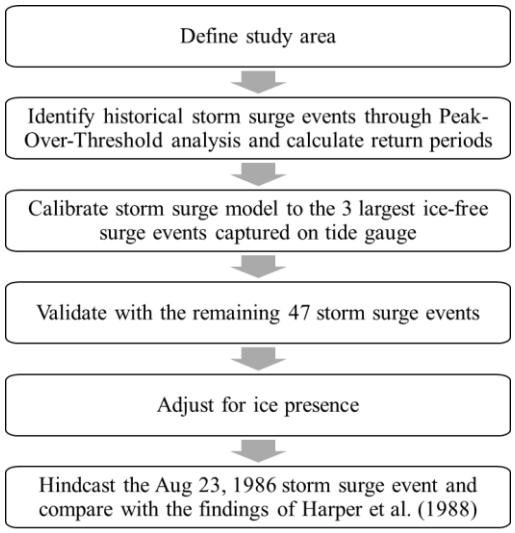

Figure 2: A high-level overview on the study's methodology

3.2.1 Study Area

The domain of the numerical model (shown in Figure 3) was selected to resemble the approximate extent of open water during minimum sea ice conditions. As the storm surge simulations performed in this study are not limited to a single state of ice condition, this methodology ensures that there is sufficient fetch to capture the development of storm surges due to wind shear stresses and changes in barometric pressure. Monthly ice records for the Beaufort Sea during the period of 1979 to 2019 were collected from the National Snow and Ice Data Centre (NSIDC) (Fetterer et al., 2017) and were used to determine the minimum ice extent that occurred during that time period. The numerical domain captures major communities that lie near the Beaufort Sea and Amundsen Gulf and extends to offshore depths of more than 3700 m.

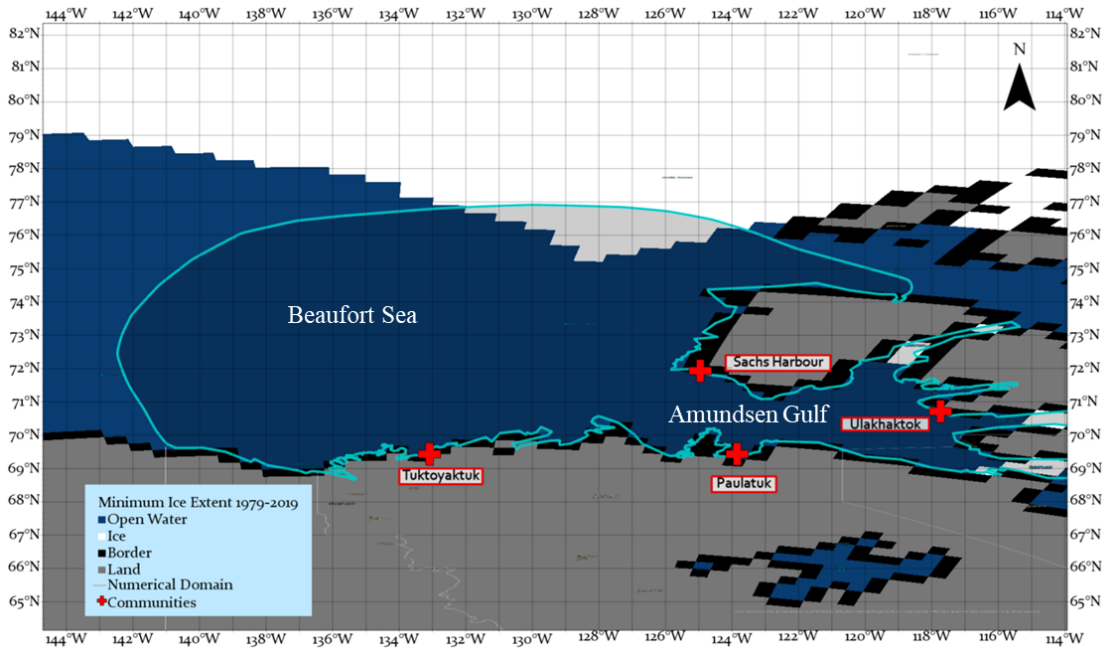

Figure 3: Numerical domain used for the storm surge model overlaid on the minimum sea ice extent during the period of 1979-2019.

3.2.2 Numerical Model

A hydrodynamic model developed in TELEMAC-2D (Hervouet and Ata, 2019) was used to model storm surges in the Beaufort Sea. The model is forced by spatially and temporally varying wind and atmospheric pressure and solves the two-dimensional depth averaged Navier-Stokes equations (Saint-Venant shallow water equations). An unstructured mesh was used comprising of 1.4 million elements with varying edge lengths of 500m (nearshore) and up to 50km (deep water). The bathymetry data was obtained from the General Bathymetric Chart of the Oceans (GEBCO) dataset (International Hydrographic Organization, 2019), which provides an interpolated grid with a resolution of roughly 500m . The 2019 version of the GEBCO bathymetry dataset was interpolated onto the unstructured mesh and is shown in Figure 4.

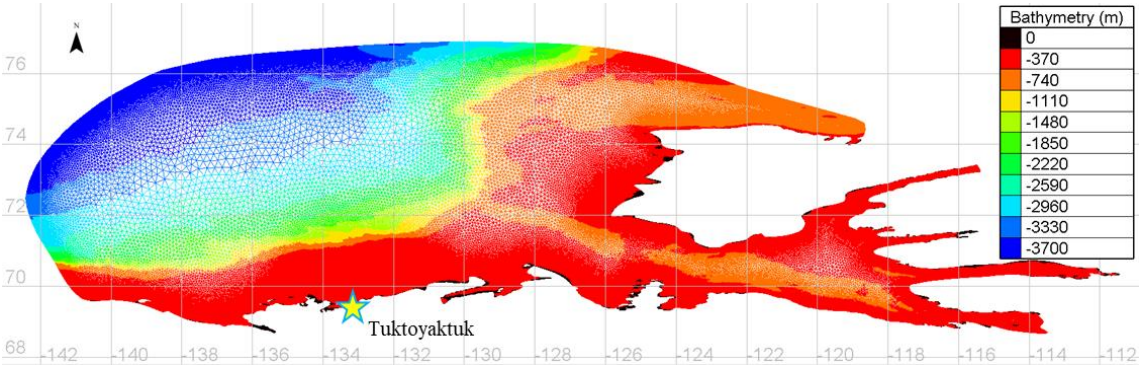

Figure 4: GEBCO bathymetry data interpolated onto the unstructured mesh used in the numerical model.

GEBCO strives to deliver a comprehensive bathymetry tied to the mean sea level (MSL) datum; however, since it is an amalgamation of multiple bathymetry datasets, some of the datasets in shallow waters may not be tied to MSL (International Hydrographic Organization, 2019) and this is noted as a potential source of error. The shoreline digitization was obtained through Open Street Maps (Topf, 2019).

3.2.3 Data Sources

3.2.3.1 Tide Gauges

Stations that record water levels in the study area are operated by the Canadian Department of Fisheries and Oceans with measurements that can be traced back to the 1960s. However, while many temporary gauges exist, long-standing records of the water level in the Beaufort Sea are exceptionally rare. Among the tide gauges in the numerical domain, the station at Tuktoyaktuk (Gauge 6485) possesses the longest-standing and most complete measurements of water levels. Thus, the Tuktoyaktuk gauge was used as the primary gauge throughout this study to support model calibration and validation. The station's water levels are reported in the local chart datum (CD)—the offset between CD and MSL for Tuktoyaktuk was calculated to be 0.454m for the mean epoch of 2010.120. All measurements reported in this paper are referenced to the local CD at Tuktoyaktuk unless otherwise specified.

3.2.3.2 Harmonic Analysis

Using the procedures outlined in Foreman et al., (2009), harmonic tidal analysis was employed to generate a predicted tidal time series based on tidal constituents developed by the Canadian Hydrographic Service (CHS). The predicted tidal elevations were then subtracted from the measurements recorded by the Tuktoyaktuk gauge, leaving only the water level residuals which are assumed in this study to be the storm surge elevations generated from wind and atmospheric pressure set-up. To account for the non-stationarity present in the residuals due to relative sea level rise, the results were de-trended by removing the slope of the best fit line about the first data point. Figure 5 shows the raw sea level elevations, the predicted tidal levels and the de-trended surge values in proceeding order.

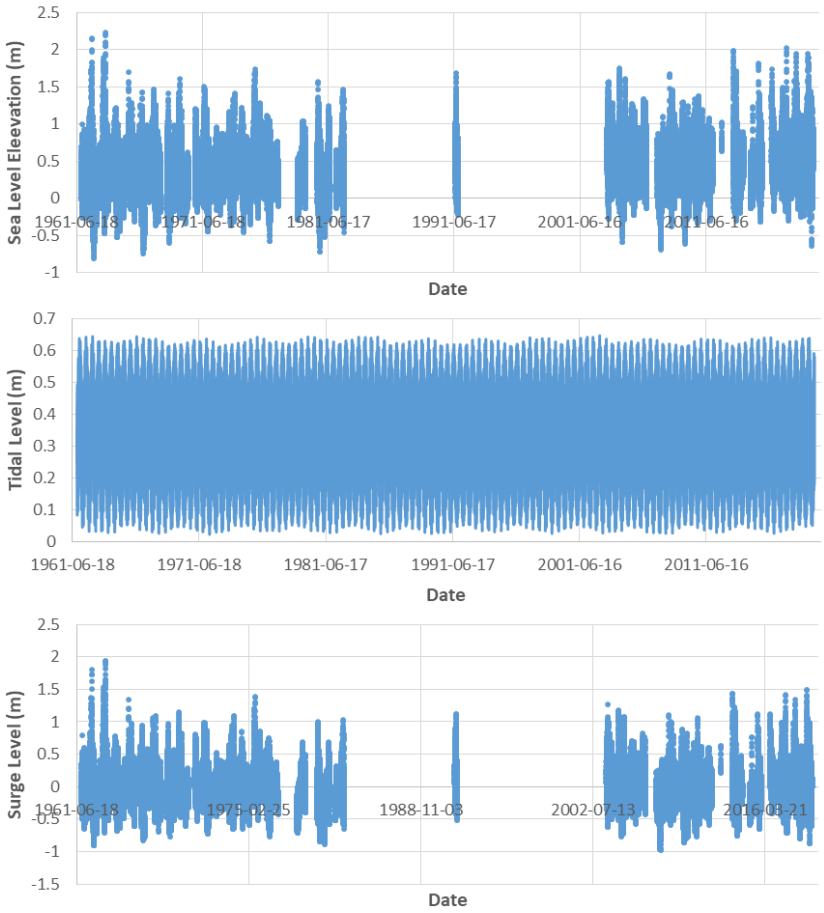

Figure 5: Station 6485 - Tuktoyaktuk a) The recorded sea level elevation b) The predicted tidal level through harmonic analysis c) The extracted residuals

3.2.3.3 Extreme Value Analysis

The largest fifty positive storm surge events were identified through extreme value analysis using the Wave Analysis and Fatigue and Oceanography (WAFO) toolbox (Brodtkorb et al., 2000). A peak-over-threshold approach was applied on the surge level time series to identify significant surge events. The identified events were then fit to a Generalized Pareto Distribution (GPD) to estimate return period magnitudes. Extreme events that occurred within a 48-hour time period of each other were counted as a single event. Figure 6 shows the fitted GPD with 95% confidence intervals.

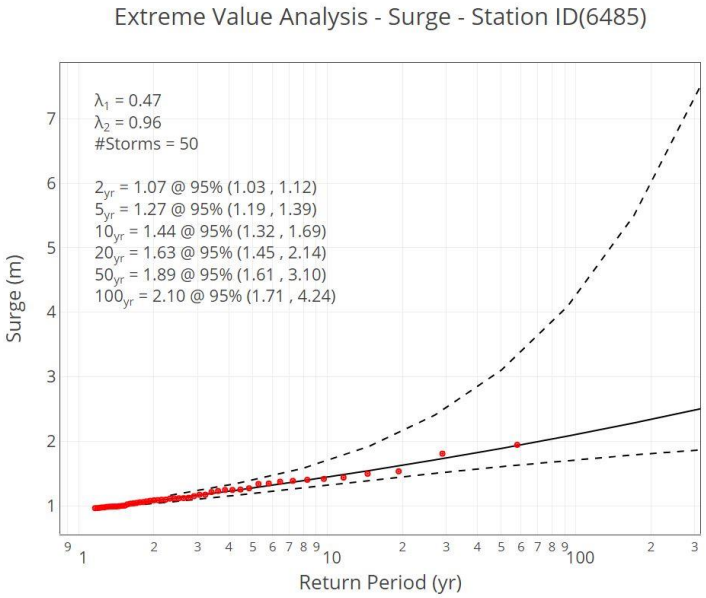

Figure 6: Return periods for the recorded storm surge events on the Tuktoyaktuk gauge.

It should be noted that even though the Tuktoyaktuk gauge is the most complete tide gauge in the study area, there are long periods where the gauge was not operational and was not able to capture large surge events (Figure 5). In particular, the events that occurred on September 1, 1944 and September 14, 1970 were not captured. Interviews with the local residents of Tuktoyaktuk estimated that these events saw water levels of approximately 3m above MSL (Department of Public Works, 1971). However, these approximations were based off of the memory of the local residents. Harper et al., (1988) found that these events produced peak water levels closer to 2.5m (MSL) based

on their field investigation of driftwood deposits, which exceeds all of the water level measurements present in the Tuktoyaktuk tide gauge record as seen in.

Table 1.

Table 1: The ten largest water levels recorded on the gauge and the two largest water level values estimated by Harper et al., (1988). Bolded events are from driftwood observations. Note that these values are in CD.

Rank	Datetime	Water Level (m)
1	**1944-09-01**	**2.95**
1	**1970-09-14**	**2.95**
3	1963-10-04 14:00	2.23
4	1962-09-04 11:00	2.15
5	2017-11-04 9:00	2.02
6	2013-09-01 6:00	1.96
7	2018-08-17 16:00	1.95
8	2019-07-21 9:00	1.94
9	2018-09-01 13:00	1.89
10	1963-07-30 11:00	1.85
11	2015-08-27 21:00	1.82
12	1962-09-01 0:00	1.78

The extreme value analysis was repeated to examine the significance of the events estimated from the driftwood lines. Harper et al., (1988) noted that their measurement of the driftwood lines is bound by a +/- 0.3m error. This error is compounded by the fact that the time of the event is not known, thus the tidal stage could vary between the daily minimum and maximum. The events from 1944 and 1970 were taken into account in the extreme value analysis at varying levels of error (i.e. the maximum surge would occur with a +0.3m measurement error and is compounded with the minimum predicted daily tidal level). The results of the extreme value analysis can be seen in Figure 7. The results show that the return period storm surge estimates change significantly with the inclusion of the estimated events.

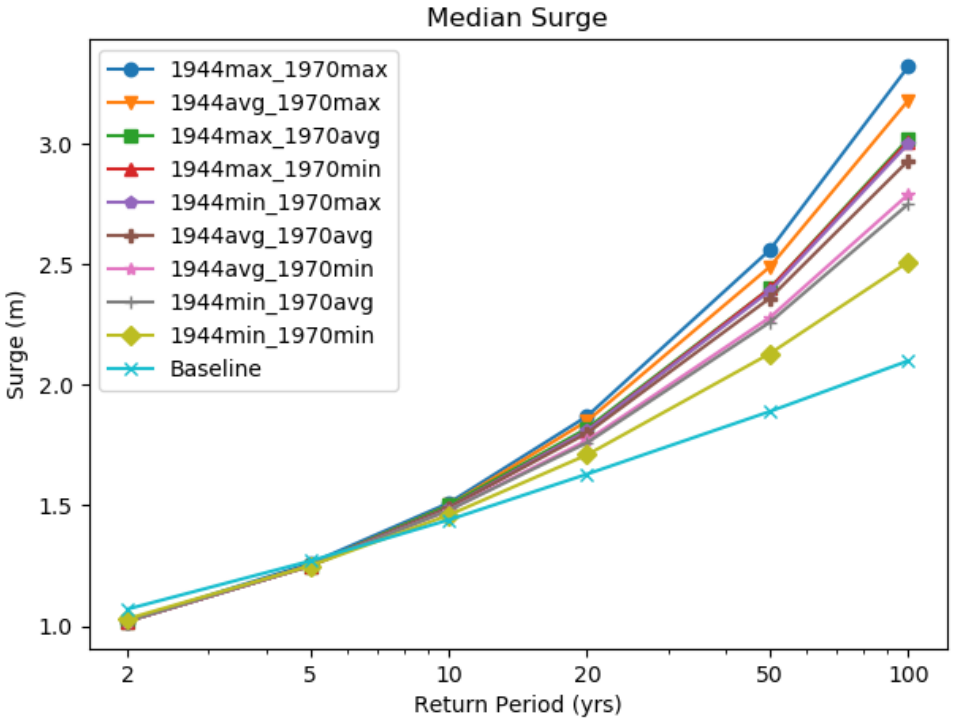

Figure 7: Effect of the events estimated by Harper et al., (1988) on the return period of surge events for varying levels of error.

The baseline 100-yr return period surge magnitude was estimated to be 2.1m when accounting only for the surge events captured by the gauge. Including the estimates for the 1944 and 1970 storm surge events, the surge magnitude associated with the 100-yr return period event increases to a minimum value of 2.5m (1944min_1970min) and a maximum value of 3.4m (1944max_1970max). While no risk analysis is performed in this study, future investigations should consider the effects of non-traditional water level sources when data sources are scarce as they may significantly impact the level of risk assigned to surge events.

3.2.3.4 Reanalysis Dataset

The ERA5 reanalysis dataset (Hersbach et al., 2020) was downloaded from the Climate Data Store. Downloaded data included hourly wind and surface pressures during the period of 1979 to 2019. As the time period of the reanalysis dataset is more constrained than the tide gauge, only surge events that fall within ERA5's time period were simulated. For context, the 50th largest storm simulated in this study is equivalent to the 89th largest storm captured on the gauge. The horizontal resolution of the reanalysis dataset is roughly 30 km.

The wind and surface pressure values of the ERA5 dataset were compared with measured values from weather stations located in Tuktoyaktuk to verify the quality of the reanalysis in the vicinity of the model domain. Five weather stations (i.e. Stations 1699, 1700, 26987, 53581, 53582) that are in close spatial proximity have been operated in Tuktoyaktuk by Environment and Climate Change Canada (ECCC) and have collected data starting from 1958. These stations have varying measurement frequencies; Station 1699 took measurements every six hours from 1958 to 1993, and the frequency increased to every hour from 1994 onwards through Station 26987. In addition to these two stations, Station 1700 was operational between 1970 and 2015 and took hourly measurements between 6 am and 10 pm (Mountain Standard Time). Stations 53581 and 53582 also recorded hourly measurements starting from 2015. Due to the overlaps in measurement periods between the weather stations, the comparisons between the ERA5 reanalysis and the measured weather data are performed using data from the weather station that had the highest measurement frequency during the selected storm surge event.

Figure 8 shows the comparison between the atmospheric pressure recorded at the weather station and the pressure field estimates provided in ERA5.

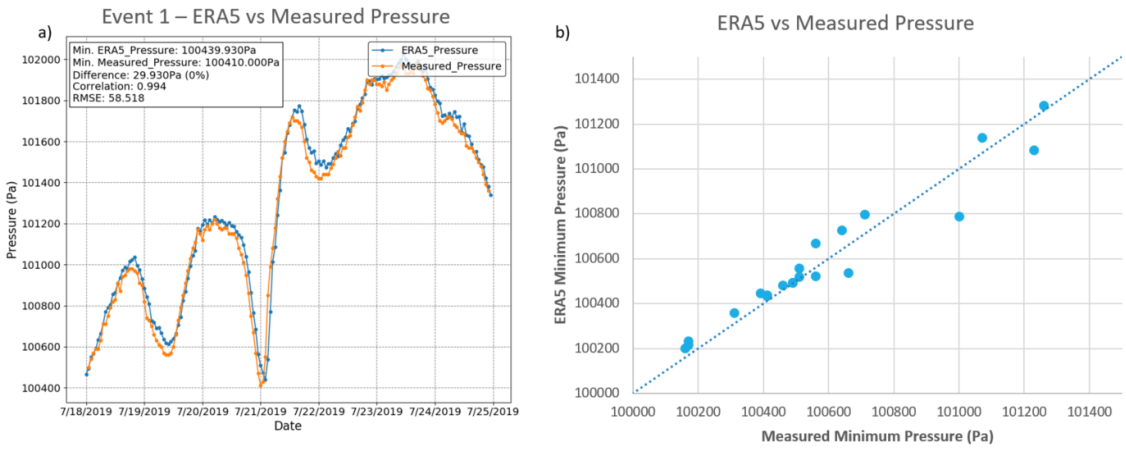

c)

	Correlation		RMSE		% Difference between Minimums	
	Mean	StDev	Mean	StDev	Mean	StDev
Pressure (Pa)	0.996	0.003	76.669	20.938	0.023	0.068

Figure 8: The performance of ERA5's pressure reanalysis: a) A direct comparison of the surface pressure field for the largest simulated surge event (July 2019); b) Measured vs. modelled minimum surface pressures for all 50 surge events; c) The mean and standard deviation for the correlation, root-mean-squared-error (RMSE), and % difference between minimums for all fifty surge events.

ERA5 pressure data showed good agreement with the atmospheric pressures recorded at the weather station. Comparison between the two datasets produced a high correlation value of 0.996, a RMSE of 77 Pa, and less than a 1% mean difference between minimum pressures for all fifty surge events. Low standard deviations were also found for the aforementioned values. As a rule of thumb, a change in 100 Pa causes a sea level difference of around 1 centimetre (World Meteorological Organization, 2011) which is a reasonable amount of error considering the storm surges in this study are on the scale of two orders of magnitude greater.

Figure 9 shows the comparison between the wind speed recorded at the weather station and the surface wind speed estimates provided in ERA5.

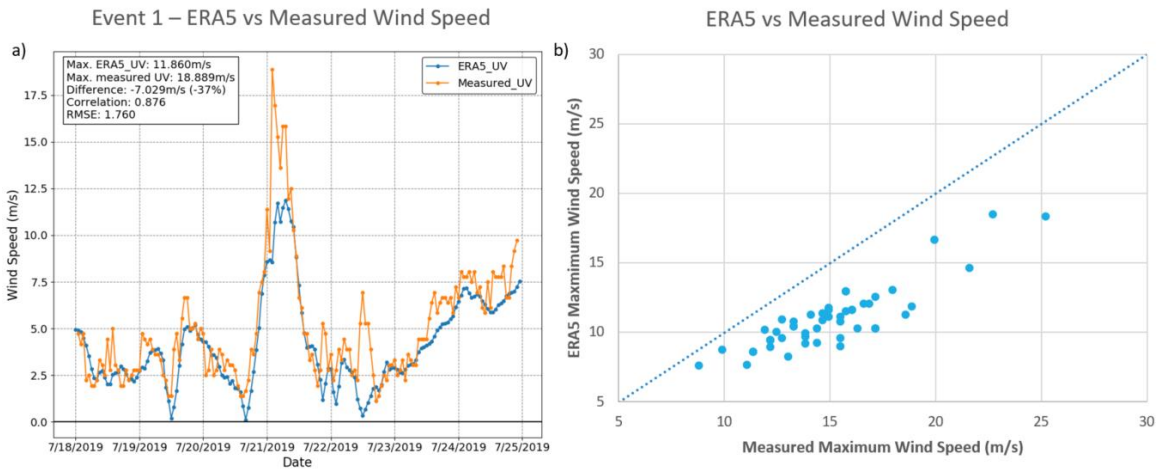

c)

	Correlation		RMSE		% Difference between Maxes	
	Mean	StDev	Mean	StDev	Mean	StDev
Wind Speed (m/s)	0.859	0.066	1.919	0.421	-26.882	7.380

Figure 9: The performance of ERA5's wind speed reanalysis. a) A direct comparison of the surface wind field for the largest simulated surge event (July 2019) b) Measured vs. modelled maximum wind speeds for all 50 surge events c) The mean and standard deviation for the correlation, root-mean-squared-error (RMSE), and % difference between maxes for all fifty surge events.

Contrary to the pressure field, wind speeds were not well captured in the ERA5 reanalysis, most notably during peak wind periods. Plotted alongside the wind speed measurements from the weather station (Figure 9b), it is evident that ERA5 consistently under-predicts the peak wind speed by an average of 27%. This held true for events that had hourly wind speed measurements and for six-hourly measurements.

3.3 Results

3.3.1 Sensitivity Study

A sensitivity study was conducted prior to the calibration of the storm surge model to assess model sensitivity of peak storm surge to mesh resolution and computational time step. Two spatial resolutions of the unstructured mesh were used in the sensitivity analysis; 3.1 million element mesh with edge lengths ranging from 50km offshore to 200m nearshore and a 1.4 million element mesh with edge lengths ranging from 50km offshore to 500m nearshore. The largest five surge events were simulated using both mesh resolutions tested, and the results of the largest surge event (July 2019) are provided in Figure 10.

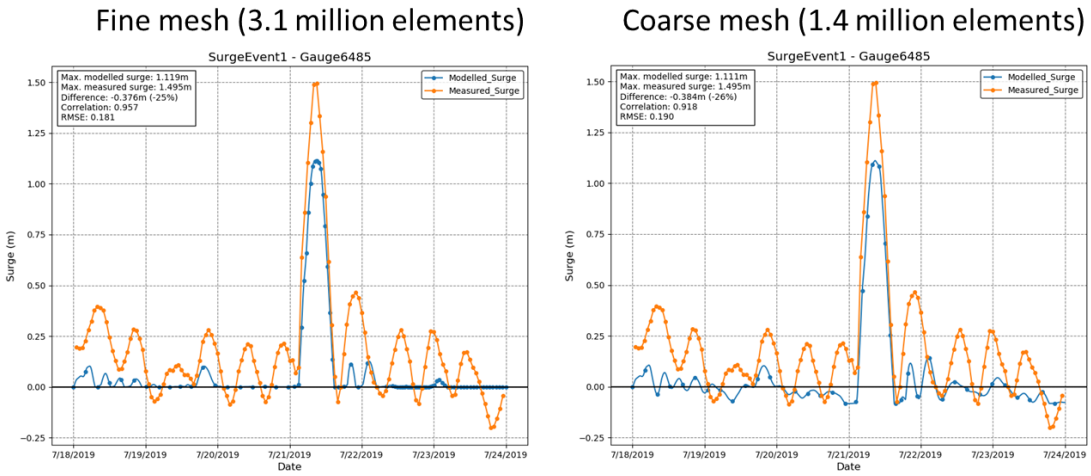

Figure 10: Mesh resolution sensitivity results for Event 1 (July 2019); 3.1 million element mesh (left) and 1.4 million element mesh (right).

A minor 1% difference in the modelled peak surge was observed for all five storm surge events, thus the coarser 1.4 million element mesh was used for the proceeding simulations. The sensitivity of the model to the time step was analyzed by comparing a constant 30s time step to a variable time step of up to 300s. In the latter case, the TELEMAC-2D software selects the computational time step based on Courant-Friedrich-Lewy (CFL) criteria specified by the modeller; in this case, a CFL condition of less than 0.9 was maintained during the simulation. Figure 11 shows an example

result of the computational time step sensitivity test for storm surge Event 4 (August 2019).

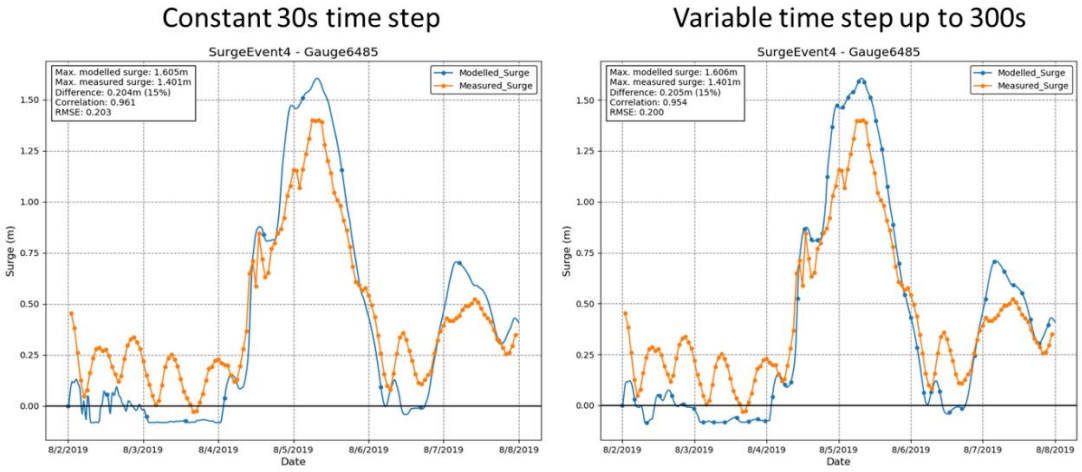

Figure 11: Computational time step sensitivity results for Event 4 (August 2019): constant 30s time step (left); and variable time step where the CFL condition is less than 0.9, and a maximum time step of 300s (right).

Minor differences in peak modelled surge, correlation, and RMSE were observed, thus a variable time step was used for the remainder of the simulations. Computational time ranged from 2 days to 8.5 days when simulating all fifty storm surge events on the six cores of an Intel Core i7-8850H processor using the coarse mesh with a variable time step and the fine mesh with a constant 30s time step, respectively.

3.3.2 Calibration and Validation

The storm surge model was calibrated by adjusting the wind drag coefficient (C_d) while keeping a constant Manning's roughness of 0.025 $s/m^{1/3}$. Three large storm surge events that occurred during the summer months (i.e. July 2019, August 2018, and September 2013) were investigated during the calibration exercise. These events were found to be ice-free around the vicinity of Tuktoyaktuk after examining the weekly ice charts from the Canadian Ice Service (CIS). This ensures that the model performs optimally when the fetch is clear of ice and allows adjustments for the influence of ice cover afterwards. The default C_d was based off of the findings of Flather (1976) and was adjusted until

good agreement was achieved between the modelled and measured storm surge for all three events. The final values used in the calibrated storm surge model are shown in Figure 12.

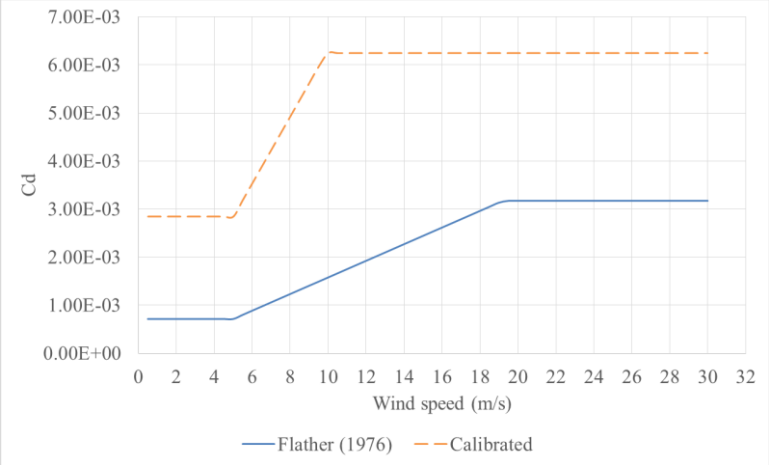

Figure 12: The final Cd values used for the storm surge model compared with the baseline values found in Flather (1976)

Due to ERA5's inability to accurately capture peak wind speeds, C_d values higher than those found in literature (Bryant and Akbar, 2016) were required to achieve good model performance. Figure 13 shows the results of the three ice-free surge events after the calibration.

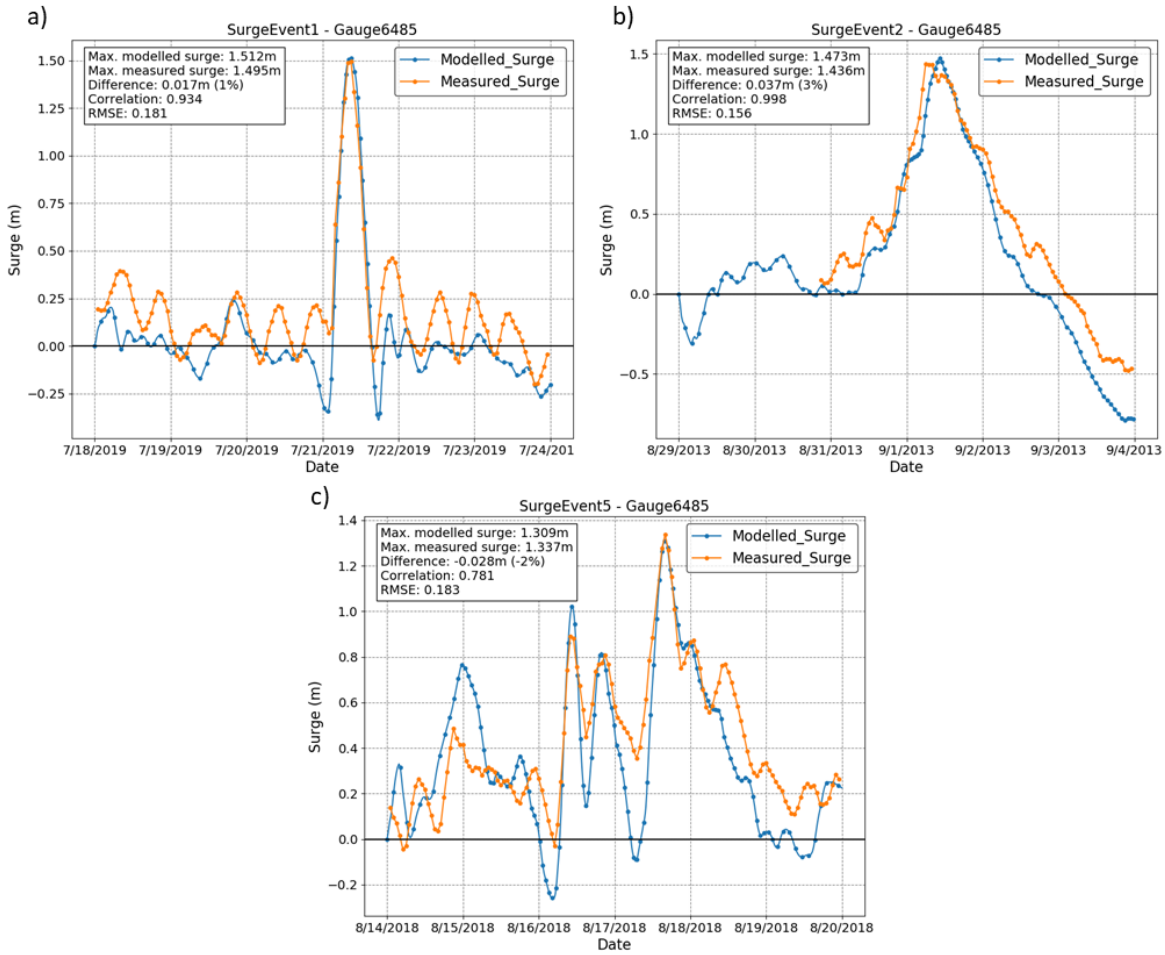

Figure 13: Sample results of the storm surge model calibration exercise for storm surge events that occurred on a) July 2019 b) September 2013 c) August 2019.

In all three events, the peak surge was modelled within a 3% difference and the duration of flooding was well captured. The remaining 47 historical events were then simulated to validate the performance of the model. Figure 14a shows the performance of all fifty storm surge events that were simulated with the calibrated model.

a)

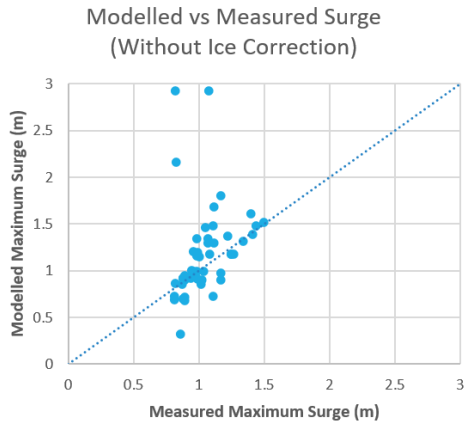

b)

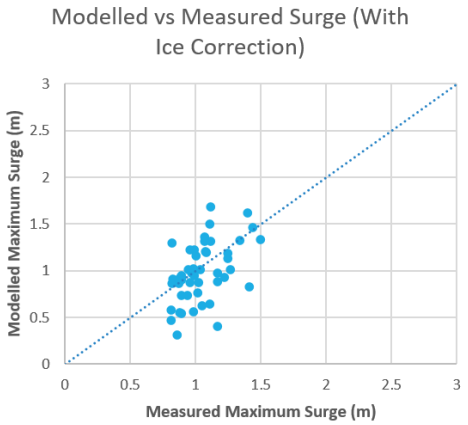

c)

	Correlation		RMSE		% Difference between Maxes	
	Mean	StDev	Mean	StDev	Mean	StDev
Storm Surge Hindcast without Ice (m)	0.821	0.200	0.327	0.232	13.715	51.539
Storm Surge Hindcast with Ice (m)	0.835	0.211	0.285	0.116	-6.550	26.155

Figure 14: a) The comparison of measured and modelled storm surge values without any corrections for ice. b) The comparison of measured vs modelled storm surge values after correcting for the effects of ice as per Joyce et al., (2019). c) The correlation, RMSE, and % difference between maximum values for each model.

While the majority of the fifty events performed well, several outliers were observed where the modelled storm surge was much greater than the measured storm surge. These events occurred during the months of December and January when fast ice can be seen on the shorelines along the north coast of Canada.

3.3.3 Effect of Ice Presence on Storm Surge

The presence of ice has been known to dampen the magnitude of storm surges by acting as a barrier between the water surface and the storm winds (Murty and Polavarapu, 1979). Conversely, during ice cover conditions with low ice concentrations, storm surges can be amplified due to the increased roughness of the ocean surface (Birnbaum and Lüpkes, 2002). Joyce et al. (2019) performed a numerical investigation on storm surges in western Alaska and proposed the following formulas to account for the effect of ice:

$$C_d = (1 - AF)C_{d-w} + (AF)C_{d-is} + C_{d-if} \quad (1)$$

Where AF is the area fraction of ice coverage which can range from 0 to 1; $C_{d\text{-}w}$ is the air-sea drag coefficient; $C_{d\text{-}is}$ is the contribution of ice skin drag and is set to a constant value of 0.0015 based on the findings of Lüpkes et al., (2012); $C_{d\text{-}if}$ is the form drag contribution from the ice based on a function of AF (Lüpkes et al., 2012):

$$C_{d-if} = 4C_{d-if,max}(AF)(1 - AF) \quad (2)$$

Where $C_{d\text{-}if,max}$ is the maximum value of $C_{d\text{-}if}$ which occurs at 50% ice coverage. $C_{d\text{-}if,max}$ was set to be 0.0025 (Joyce et al., 2019). These formulas were incorporated into the calibrated model with ice presence sourced from the weekly ice charts issued by CIS. Figure 15 shows a comparison between one of the outlier events, Event 18 (that occurred during January 2005), where heavy ice presence and fast ice were found near Tuktoyaktuk.

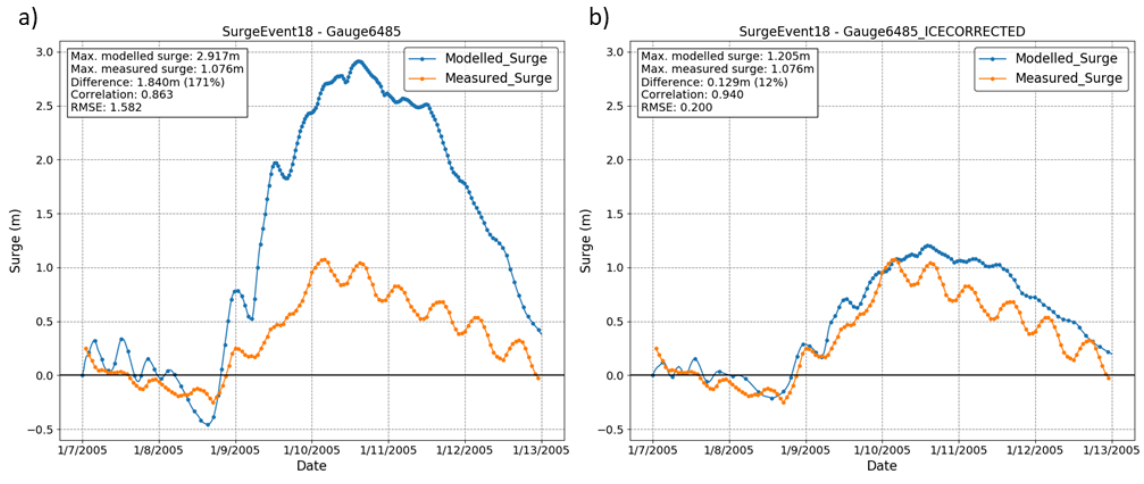

Figure 15: Comparison of modelled and measured storm surge elevations for Event 18: a) Before accounting for the presence of ice. b) After accounting for the presence of ice.

The storm surge model originally over-predicted the peak storm surge by 171%, but was reduced to a 12% over-prediction after accounting for the presence of ice. These findings suggest that sea ice plays a significant role in reducing peak storm surges during winter months. As sea ice extent and duration continue to decline in the Arctic (Barnhart et al., 2016), it is reasonable to expect that future winter storm events could, in general, produce greater storm surge magnitudes than those observed today. Figure 14b shows a comparison of the measured and modelled storm surges after accounting for the presence of ice—the outliers that were present in the original model results have been reduced. In addition, Figure 14c shows that the numerical model has higher correlation, and lower RMSE and % difference between peak surge values after accounting for the presence of ice.

3.3.4 Hindcast of the August 23, 1986 Storm Surge Event

Harper et al. (1988) estimated maximum water levels based on field observations of driftwood lines for a significant event that occurred on August 23, 1986. This event was not captured on the Tuktoyaktuk (6485) tide gauge and was simulated to further validate the storm surge model. The simulation included the influence of sea ice as described in Section 3.3. Near Tuktoyaktuk, Harper et al., (1988) estimated maximum local water level of approximately 2.1m (converted from MSL to CD). The predicted tide level during August 23, 1986 (calculated from the analysis described in Section 3.2.3.2) was subtracted from the estimated water levels to yield only the storm surge component. A minimum tide level of 0.16m and a maximum tide level of 0.52m was predicted for August 23, 1986. This provides an estimated storm surge level ranging from 1.53m to 1.90m depending on the tidal level during the storm, compounded by the +/-0.3m of measurement error noted by Harper et al (1988). Figure 16 shows the simulated storm surge elevations for a study area similar to the study area of Harper et al. (1988).

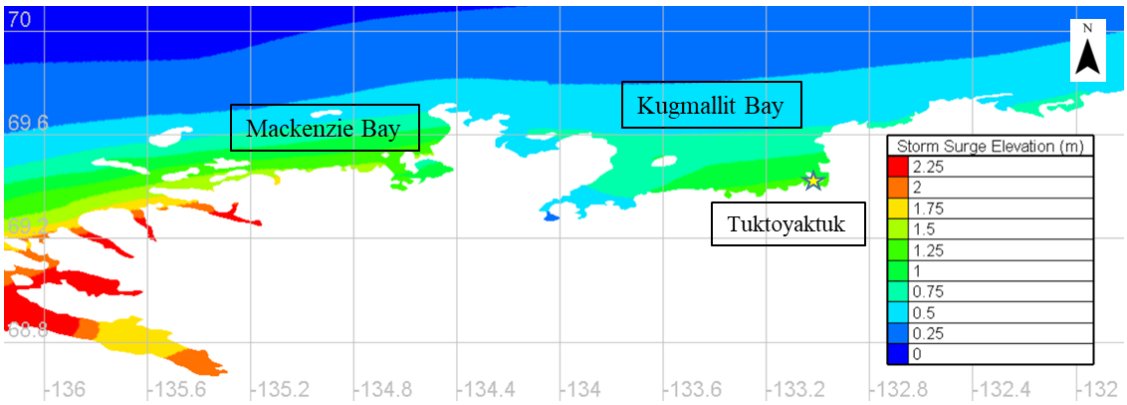

Figure 16: Hindcast of the August 23, 1986 event.

The simulated local maximum surge near Tuktoyaktuk was found to be approximately 1.4m, which falls within the bounds of the estimation provided by Harper et al., (1988) after considering their expected measurement error (1.53m to 1.90m +/- 0.3m). This numerical exercise lends confidence to the use of driftwood lines to estimate elevated water levels produced by storm events where no measured data exists and, concurrently, to the estimates proposed by Harper et al. (1988) describing maximum water levels of up to 2.95m that have occurred in Tuktoyaktuk region within the past 100 years.

The model results showed good agreement with the estimates provided by Harper et al. (1988), despite some discrepancy between the climatic forcing data from ERA5 reanalysis and the recorded measurements from a nearby weather station (see Figure 17).

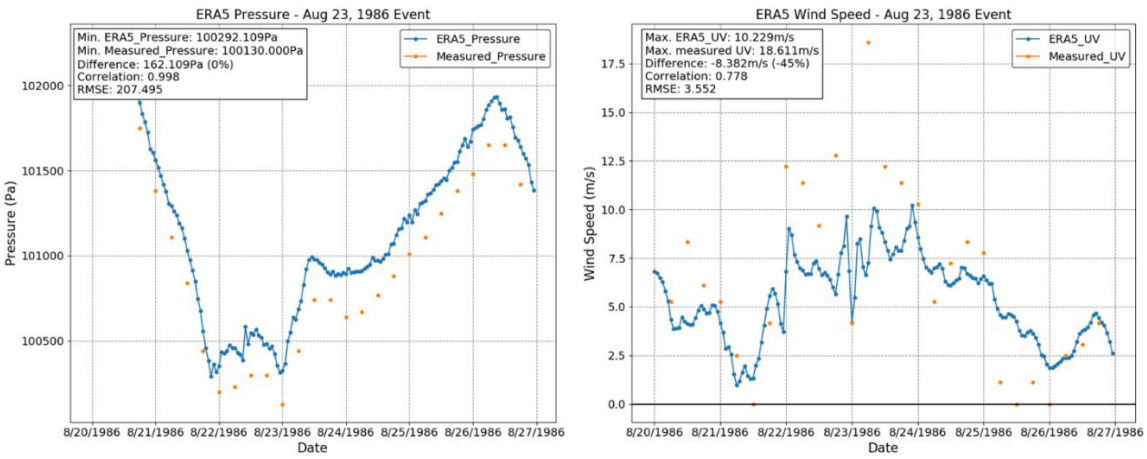

Figure 17: Surface pressure and wind fields for the August 23, 1986 event approximated in the ERA5 reanalysis and measured by weather station 1699 located at Tuktoyaktuk.

While the pressure field was closely tracked by the ERA5 reanalysis with a RMSE of 207 Pa, the ERA5 wind reanalysis did not capture the peak wind speeds that were recorded by the weather station at Tuktoyaktuk. The six-hourly measurements show that the ERA5 reanalysis under-predicted the peak wind speed by 45% (8.4 m/s). Despite these discrepancies, the calibrated model yielded storm surge elevations similar to the estimates provided by Harper et al., (1988).

3.4 Discussion

3.4.1 Quality of the ERA5 Dataset

The advancement in global climate modelling has led to the development of high-resolution reanalysis datasets such as ERA5. Among the many climatic variables that these datasets offer, surface pressure and wind have been used in storm surge models as a forcing input. Previously, ERA5 has been shown to be a large improvement over its predecessor, ERA-Interim, when used in storm surge models focused on the Pacific and Atlantic coastlines (Dullaart et al., 2020; Muis et al., 2020). This study examined the performance of ERA5 in the Arctic regions of Canada and its potential use in hindcasting storm surge events. The ERA5 dataset demonstrated a high level of skill when tracking surface pressure, with a less than 1% mean error in minimum pressure

among the fifty storm surge events that were studied. However, the ERA5 reanalysis was not able to accurately capture peak wind speeds and under-predicted them by 27% on average with a standard deviation of 7%. This can yield low estimates of modelled storm surges as the momentum transfer between the air and sea is under-approximated. This study compensated for the under-predicted wind speeds by using wind drag coefficients larger than those commonly found in literature (Bryant and Akbar, 2016). Promising results were obtained when validating the storm surge model with fifty historical surge events captured on the Tuktoyaktuk tide gauge and through hindcasting a historical event with peak surge levels estimated through driftwood deposits.

3.4.2 Quality of Historic Tide Gauge Records and Impacts on Uncertainty

Extreme value statistics are often employed to describe the likelihood or reoccurrence-interval of natural phenomenon that, otherwise, cannot be easily described deterministically. The quality of extreme value analyses is intrinsically linked to the quality of the data records available to inform statistical computations.

In this study, return period estimates for peak storm surge magnitude were determined based on water level records available from the Tuktoyaktuk tide gauge. As discussed in Section 2.3, the tide gauge has a rather long period of record, dating back to 1961. However, the gauge record is interrupted by periods of inactivity where the gauge was not operational. Most notably, the tide gauge record does not include two recent high-water-level events that occurred in 1944 and 1970, for which Harper et al. (1988) estimated sea-level elevations exceeding any elevation present in the tide gauge record. It is uncertain whether these high-water events occurred during a low, mid, or high tidal stage. Therefore, it is not possible to elucidate a single storm surge magnitude for the two events and rather, a range of possibilities exist. However, even conservatively-low estimates for storm surge magnitude for the 1944 and 1970 events exceed the maximum surge estimated from the tide gauge record; assuming the highest tidal stage, and considering the largest measurement uncertainty cited by Harper et al. (1988), surge

magnitude estimates for both the 1944 and 1970 events equate to ~2.1m. The maximum storm surge estimated from the tide gauge record is equal to 1.94m. This suggests that the 1940 and 1970 events are not only statistically significant, but are likely amongst the largest of storm surge events to have occurred in Canada's western Arctic region in recent history. As such, the inclusion, or non-inclusion, of these events in extreme value analyses has a significant impact on reoccurrence-interval or return period estimates.

This study has demonstrated methods to incorporate alternative sources of coastal flood evidence (driftwood debris observations) into extreme value analyses, in lieu of complete and continuous tide gauge measurements. Accounting for uncertainty associated with measurement accuracy and event timing, a range of statistical distributions describing storm surge likelihood are presented. The results indicate that 100-year return period surge magnitudes could exceed baseline estimates by as much as 1.3m. The presented methods and techniques may be of value to coastal flood practitioners working in locations where there is knowledge of large coastal flood events that are not captured in tide gauge records.

3.4.3 Considerations Pertaining to Ice Cover and Future Climatic Trends

Storm surges occur year-round under varying levels of ice presence in the Beaufort Sea. The use of the formulas presented by Joyce et al. (2019) to account for the effect of ice on storm surges in western Alaska saw good results for the events simulated in this study. The adjustments correctly dampened the over-predicted modelled storm surge elevations for winter events where fast ice is present in the vicinity of Tuktoyaktuk (Figure 14). While the winter storm surge events presented in this paper were not seen to be among the largest storm surge events captured on the gauge, Figure 15 shows that significantly higher magnitudes of surge may be seen as less ice cover is present to reduce the air-sea stress transfer during stormy periods. This is especially important as the Arctic region has been known to be the hotspot of climate change impacts. The open water season is predicted to increase, with lower ice concentrations and declining ice-

cover extents (Barnhart et al., 2016). The typical open-water season of June to October along the north coast is predicted to lengthen to a season spanning April to December by 2100 (Manson and Solomon, 2007). In addition to the changes in ice conditions, the maximum relative sea level rise is estimated to be around 1m by 2100 under the RCP8.5 scenario for the Tuktoyaktuk region (James et al., 2015). The relative sea level rise is exacerbated by the increasing permafrost temperatures (Ford et al., 2018) which can lead to retreating coastlines (Hoque et al., 2017). Storminess and extreme wind events are thought to see a decrease in frequency, with a slight increase in peak wind speed (Manson and Solomon, 2007). However, there has been some evidence showing that atmospheric patterns may not conform to a linearly increasing trend, but rather a cyclical shift between circulation that can cause significant changes to atmospheric parameters (Atkinson, 2005). These factors can increase the impacts storm surges and future studies that forecast storm surges under various climate change scenarios and ice conditions may be useful for the community planners along the north coast.

3.4.4 Limitations and Research Needs

The formulas presented by Joyce et al., (2019) consider only the effect of the presence of ice on storm surges. However, the type of ice can be a significant factor on its effect on the propagation of long waves. Fast ice dampens waves more than floating ice and the thickness of ice can also influence the degree of damping (World Meteorological Organization, 2011). In addition to the formulations, improvements in the inputted data can be achieved by using the daily ice charts issued by CIS. However, available daily ice charts span a smaller temporal range compared to the weekly charts, and daily ice charts are not issued during the winter months, limiting the number of potential storm surge events that can be investigated.

The storm surge model used in this study did not consider the effect of tides and wave run-up. While the effects of tides may be negligible due to Tuktoyaktuk's (and neighbouring areas) micro-tidal environment (Henry and Heaps, 1976), the effects of

wave set-up may have an impact on the storm surge levels predicted by the numerical model. In addition, it has been shown that waves can increase the surface roughness of the ocean, which in turn enhances the momentum transfer due to wind stresses (Johnson & Højstrup, 1998).

While this study focused on the use of ERA5 reanalysis as the source of climatic forcing data, ERA5 is one of many reanalysis datasets that also offer climate variables. The quality of other reanalysis datasets such as the Japanese 55-year reanalysis (Japan Meteorological Agency, 2013) and the MSC Beaufort Wind and Wave Reanalysis (Swail et al., 2007) were not investigated. The latter is particularly interesting as it has a higher spatial resolution and is specifically concentrated on the Beaufort Sea region. However, the spatial extent of data is limited compared to the ERA5 reanalysis, and it does not provide surface pressures. Future investigations may be able to nest the MSC dataset within a more complete reanalysis dataset and investigate its use in storm surge modelling.

3.5 Conclusions

A numerical investigation of storm surges in the Beaufort Sea was conducted. A calibrated hydrodynamic model was developed to support simulation of storm surge in Canada's western Arctic region. Customized subroutines were employed to incorporate the impacts of sea ice on storm surge. Following model calibration and validation, the model was used to hindcast a storm surge event where tide gauge records are non-existent, but non-traditional records of high-water marks exist. During this process, the quality of the ERA5 reanalysis dataset was also assessed. The following conclusions were found throughout the course of this study:

- There is a lack of long and continuous records of water levels among the tide gauges in the Beaufort Sea.

- Non-traditional records show that storm surges that are significantly more severe than those captured on tide gauges have occurred.

- Without accounting for these non-traditional records, the expected return periods of storm surge events can under-approximate the level of flood risk a community may experience.

- The numerical model was in good agreement with the findings of the non-traditional records.

- The ERA5 reanalysis was shown to track surface pressures accurately during stormy periods.

- The ERA5 reanalysis was shown to consistently under-predict the peak wind speeds during stormy periods.

- Despite discrepancies in ERA5 wind speed data, acceptable numerical modelling results were achieved through calibration of the wind drag coefficient; large wind drag coefficients were prescribed to compensate for the generally low wind speeds reported in ERA5.

- The presence of ice has a significant impact on storm surge elevations and should be considered in numerical storm surge models.

3.6 Acknowledgements

This work was funded by Defense Research and Development Canada through the Canadian Safety and Security Program supported by National Research Council Canada's Marine Infrastructure, Energy and Water Resources and Ocean Program and Ioan Nistor's NSERC Discovery Grant. The authors would like to thank Nicky Hastings and Jackie Yip (Natural Resources Canada) and all other project partners for their collaboration.

3.7 Link to Chapter 4

The hydrodynamic hazard for the western Arctic region of Canada was quantified through a numerical model in Chapter 3. While this is the primary output of many hazard assessments, the results of a hydrodynamic simulation can also be used as inputs to assess other hazard parameters such as life safety. Chapter 4 switches the area of interest from the Arctic to the Pacific coastline of Canada where tsunamis are a potential source of coastal hazard and uses the results of a tsunami hydrodynamic simulation to assess the state of evacuation preparedness for a community.

Chapter 4 Technical Paper – A Comparison between Agent-Based and GIS-Based Tsunami Evacuation Simulations: A Case Study for Tofino, BC[3]

4.1 Introduction

In Japan, hard-structural tsunami mitigation measures such as the Kamaishi breakwater and other seawalls protecting the coastal areas experienced partial and often total failure during the 2011 Tohoku Tsunami (Suppasri et al., 2013). Post-tsunami field surveys and investigations indicated that additional considerations are required to improve the design of such structures such that they become safe and efficient tsunami mitigation measures. The recent major tsunami events provided researchers with rather rare opportunities to conduct field investigations which provided insight on the performance of various structural systems (Chock et al. 2013; Palermo et al. 2013; Ruangrassamee et al. 2006; Saatcioglu, Ghobarah, and Nistor 2006; Stolle et al. 2020). The results of these surveys and subsequent investigations showed that the standardization of tsunami resistant structural design is still in its infancy: as such, researchers and practicing engineers joined their effort to develop a first building standard, written in mandatory language, in the form of Chapter 6 – Tsunami Loads and Effect of the ASCE/SEI7-16 in 2017 (American Society of Civil Engineers, 2017). Additional research showed that is difficult to design and construct a physical structure to fully protect a coastal region against tsunami waves attack. This is particularly challenging due to the high cost and societal impacts involved (Shibayama et al., 2013). Thus, soft measures, such as horizontal and vertical evacuation planning, are still preferred when protecting coastal communities against the loss-of-life during tsunami inundation events.

[3] Joseph Kim, Tomoyuki Takabatake, Ioan Nistor, "A Comparison between Agent-Based and GIS-Based Tsunami Evacuation Simulations: A Case Study for Tofino, BC", In submission process.

Tsunamis pose great community challenges when designing an effective evacuation plan due to the nature of its time scale. Hazards such as earthquakes and building fires create panic among people and evacuation using consists of leaving the hazardous area. On the other hand, in the case of events such as typhoons and hurricanes, several days of prior warnings alert the residents of the soon incoming danger. Unlike the previously mentioned natural disasters, tsunami waves arrival times range from several hours (i.e. far-field earthquake events), to several tens of minutes (i.e. near-field earthquake events) (Wang et al., 2016). In conjunction with the time needed to circulate a tsunami warning from seismic detection, this creates a pressing need to develop and inform residents of an efficient tsunami evacuation plan to maximize life-safety (Katada et al., 2006).

Two methods to model pedestrian evacuation during tsunamis events are commonly found in literature: agent-based models (ABM) and static models (typically done in Geographical Information Systems - GIS). Geographic information systems (GIS) have been widely used to perform evacuation simulations due to their prowess in handling spatial datasets. Generally, GIS-based methods assess the evacuation potential based on a cost that can vary depending on the implementation method. Cova and Church (1997) utilized the least cost distance travelled along road networks for nodes that accounted for multiple evacuees. Laghi et al. (2006) created an *ArcGIS* toolbox which facilitates isotropic evacuation, meaning that their model accounts for the effect of the topographic slope on evacuation potential, but cannot differentiate whether an evacuee is moving uphill or downhill. Cheff et al. (2019) applied an anisotropic model, which accounts for the effect of slope, including the approaching direction, to assess evacuation potential for discretized zones of population. These methods are static methods and share the same disadvantage: as GIS is not able to incorporate temporal-based behaviour (e.g. interactions between evacuees during evacuation, changes in an evacuation route), evacuation simulations in GIS do not portray a realistic picture of

emergency preparedness (Brown et al., 2005). Consequently, ABMs are increasingly preferred when assessing complex evacuation processes as each agent can follow a set of rules that can reproduce a variety of complex and dynamic evacuation behaviour of an evacuee, and account at the same time for the interactions between them (Mas et al., 2015; Takabatake et al. 2017, 2018).

However, the complexity of ABM models come at a cost. As ABMs require in-depth knowledge of evacuation behaviour and specialized skills during implementation, they are more difficult to utilize to formulate an evacuation plan than GIS, which is a much more familiar program among city planners and engineers. It is thus meaningful to quantitatively compare these two tsunami evacuation modelling approaches, for a given study area. While there have been some attempts in multiple fields to integrate agent-based behaviours into GIS models and vice-versa (e.g., Jumadi et al., 2016; Liu et al., 2016; Uno & Kashiyama, 2008), to the authors' knowledge such a comparative study has never been conducted. Thus, the present study aims to investigate the differences in results between the two methodologies and clarify whether these differences are significant enough to warrant specialized expertise and extra computational power required when using ABMs.

As a study area, the authors selected the District of Tofino, a coastal community on the west coast of Vancouver Island, British Columbia (BC), Canada. This area has been recognized as an area of major hazard due to the threat of tsunami waves (Cherniawsky et al., 2007; Clague et al., 2000; Johnstone and Lence, 2012). Recently, on January 23, 2018 at 1:31am PST, a M_w 7.9 earthquake occurred in the Gulf of Alaska which prompted a tsunami warning for certain parts of the west coast of the United States and Canada (USGS, 2018). The District of Tofino first notified its residents via their mass notification system at 2:07 am PST, and the first outdoor warning sirens sounded at 2:16am PST. By 3:40am PST, most people in low-lying areas in the District had evacuated to higher ground and the evacuation order was cancelled at 4:37am PST as

no far-field tsunami was expected to reach Tofino.

This particular event shone light on the tsunami emergency preparedness for the District of Tofino. While a 2-hour evacuation period may be sufficient for distant source tsunami, previous studies showed that a M_w 9.0 earthquake from the Cascadia Subduction Zone (CSZ) may propagate a near-field tsunami to Tofino in 20 minutes (Takabatake, et al., 2019). Paired with findings of Leonard et al. (2014), where they estimate that a CSZ event that can cause significant tsunami run-up (i.e., larger than 3 m) on the west coast of Vancouver Island has probability of occurrence of 10-30 % within a period of 150-560 years, there is a need to critically assess tsunami hazard mitigation and/or adaptation methods to decrease loss-of-life during those events.

In the present study, the performance of an ABM and GIS will be assessed by first simulating the current state of tsunami evacuation preparedness for the community of Tofino, and then compare the simulated effectiveness of additional mitigation measures through the introduction of new, and expanded evacuation locations. Typically, GIS-based evacuation models define evacuees through discretized blocks of land with population densities or nodes that account for multiple evacuees as defining every single agent is thought to be impractical (Cova and Church, 1997). However, as the agents in an ABM are all geospatially referenced, in the present study it is possible to export and import the same initial locations of evacuees between the ABM and GIS. This provides a unique opportunity to assess the performance of a GIS-based evacuation model populated with individual evacuees.

The numerical investigation performed in this study uses the ABM developed in Takabatake et al. (2020c), where they performed a comprehensive tsunami evacuation simulation for the District of Tofino. The present study however adds additional interaction between agents through the implementation of the effect of crowd density on evacuation speed. The results of the updated ABM are then compared with the

results of the GIS evacuation model with a 1:1 replica of the population distribution used in the ABM used to assess the differences in performance between the two modelling strategies.

4.2 Methodology

A summary of the components of this study is shown in Figure 18.

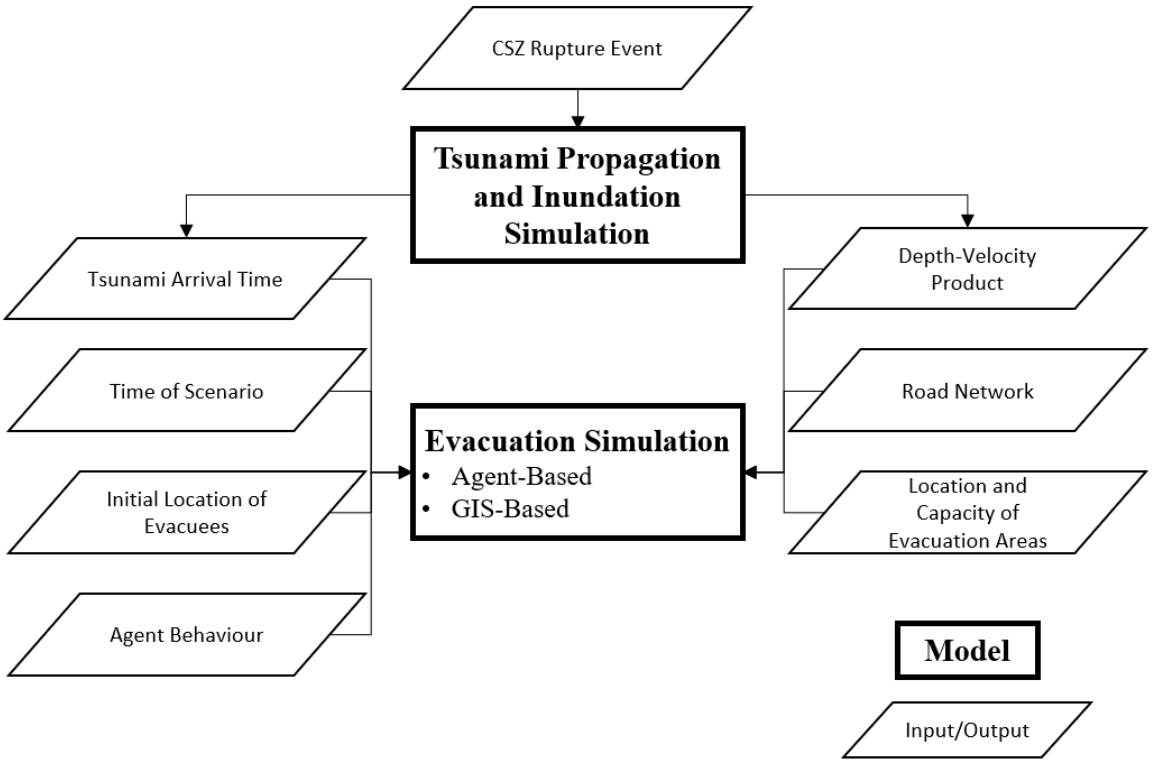

Figure 18: High-level overview of the methodology. Parallelograms denote inputs and outputs required for an evacuation model, while rectangles are the processes (model) which utilize the variables.

An earthquake scenario was first defined and used as the generation mechanism for the tsunami propagation and inundation simulation. The outputs of the hydrodynamic model were then used as inputs in the evacuation models to calculate when agents are to be considered casualties. Additional inputs for the evacuation model included: the initial population distribution of evacuees, the time of the scenario being simulated (i.e.,

daytime or night-time, summer or winter), the road network that agents can use, the behaviour of the evacuees during the evacuation, and the location and capacity of each designated evacuation location.

The agent based model was developed in *Artisoc* (Yamakage, 2009), a platform that allows the user to freely define agent behaviour using a programming language similar to *Visual Basic*. The GIS simulation model was developed based on *ArcGIS' ArcMap* using the *Network Analyst Toolbox*. *Network Analyst* is a common functionality that GIS users are already familiar with or which can be easily learned if city planners want to assess evacuation preparedness. Using the *Network Analyst Toolbox* does not require a deep understanding of agent behaviours (unlike the complex interactions that can occur in ABMs) and does not require substantial model set-up time compared to ABMs or other GIS methods. While *Network Analyst* can solve a variety of location-allocation problems, the *Maximum Capacitated Coverage* algorithm was used in the present study as it can account for an agent's cost to reach an evacuation location and limit the capacity of each location.

4.2.1 Tsunami Propagation and Inundation Simulation

Due to the proximity of Vancouver Island to the CSZ, there have been several regional studies assessing the tsunami hazard that the island faces. Clague et al. (2000) investigated the sediment deposits from a historical tsunami for multiple locations across Vancouver Island and estimated maximum run-ups through these records. AECOM (2013) numerically investigated the tsunami propagation and inundation process on the southern-western portion of Vancouver Island to model the CSZ tsunami hazard for 500-year return period events. For studies focusing on Tofino, BC, Takabatake et al. (2019b) assessed the tsunami hazard at the regional level along the entire Pacific facing coastline, and provided 20 m-resolution inundation maps for the communities of Port Alberni, Ucluelet, and Tofino. Those findings were further refined in Takabatake al. (2020c) using higher resolution DEM datasets for the District of

Tofino (with a resolution of 0.5–1.5 m). The present study directly used the high-resolution inundation results (i.e., no additional hydrodynamic modelling was performed in this study). A summary of the tsunami model used is shown in Table 2. Although three earthquake scenarios were simulated in Takabatake al. (2020c), upon discussions with the local emergency preparedness authorities of Tofino, the M_w 9.0 scenario was selected as the earthquake scenario for the present evacuation models.

Table 2: Summary of the properties of the tsunami hydrodynamic model used in Takabatake et al. (2019b). See Section 8 for variables used in governing equations.

Parameter	Value
Nested domain resolutions (m)	1620, 540, 180, 60, 20
Manning's roughness coefficient ($s/m^{1/3}$)	Constant value of 0.025 is used for 1620, 540, 180 m domains. Different values of 0.025 (ocean) and 0.030 (land) are used in the 60 and 20 m domains.
Digital Elevation Model (DEM) sources	GEBCO, CDEM, CHS, Local Data
Earthquake Moment Magnitude scenarios	M_w 8.7, M_w 9.0, M_w 9.3
Soil deformation model	Okada (1985)
Hydrodynamic model	Waseda NLSW (Takabatake et al., 2019b)
Discretization method	Leap-frog finite difference scheme (Imamura, 1997)
Governing equations (Non-linear shallow water equations)	$$\frac{\partial \eta}{\partial t}+\frac{1}{R\cos\varphi}\{\frac{\partial M}{\partial \lambda}+\frac{\partial}{\partial \varphi}(N\cos\phi)\}=0 \quad (1)$$
	$$\frac{\partial M}{\partial t}+\frac{1}{R\cos\varphi}\frac{\partial}{\partial \lambda}\left(\frac{M^2}{D}\right)+\frac{\partial}{R}\frac{\partial}{\partial \varphi}\left(\frac{MN}{D}\right)+\frac{gD}{R\cos\varphi}\frac{\partial \eta}{\partial \lambda}-fN+\frac{gn^2}{D^{\frac{7}{3}}}M\sqrt{M^2+N^2}=0 \quad (2)$$
	$$\frac{\partial N}{\partial t}+\frac{1}{R\cos\varphi}\frac{\partial}{\partial \lambda}\left(\frac{MN}{D}\right)+\frac{1}{R}\frac{\partial}{\partial \varphi}\left(\frac{N^2}{D}\right)+\frac{gD}{R\cos\varphi}\frac{\partial \eta}{\partial \varphi}+fM+\frac{gn^2}{D^{\frac{7}{3}}}N\sqrt{M^2+N^2}=0 \quad (3)$$

4.2.2 Time of Scenario and Initial Location of Evacuees

Takabatake et al. (2020c) found that the northern region of the District of Tofino would experience minimal inundation even during more extreme events (i.e., a M_w 9.3 event), and, thus, only the southern portion of the community was simulated in the evacuation models. Additionally, among the four scenarios simulated in Takabatake et al. (2020c), the two summer scenarios (daytime and night-time) were found to have higher fatality rates compared to the winter scenarios. Therefore, only the summer scenarios were simulated in the present study.

The time of scenario affects the initial location of the evacuees. For instance, more people would be located outside by the beach areas during the daytime, while during the night-time many would be staying in their resort buildings or homes. Table 2 and Figure 2 show the initial locations of evacuees used for each scenario. The total number of evacuees and the distribution of evacuees' initial locations were verified with the local authorities of Tofino and are reproduced identically in both the ABM and GIS model.

Table 3: Proportion of agents located on the beach or in a building for each scenario.

Name of scenario	% of agents on the beach	% of agents in a building	Total number of evacuees
Summer Daytime (SD)	60	40	4573
Summer Night-time (SN)	0	100	4648

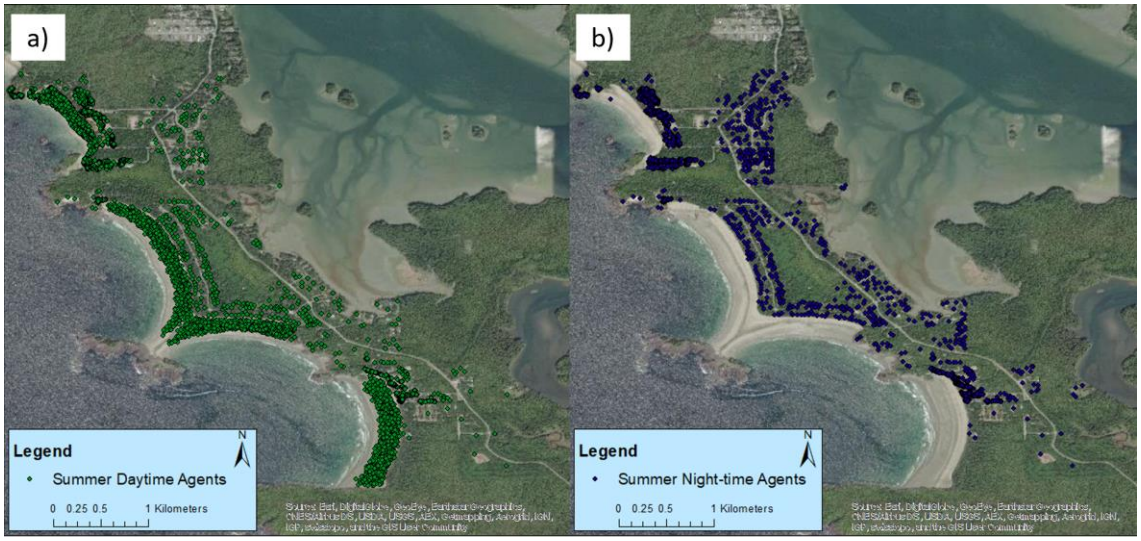

Figure 19: Initial location of evacuees used for both the ABM and GIS evacuation simulations. a) SD scenario where agents are located outside near the beach and scattered throughout the city. B) SN scenario where agents are mainly inside their homes/resort.

4.2.3 Road Network

Both models incorporated the local road network that was provided by Northwest Hydraulics Consultants (NHC) and the local authorities of the District of Tofino. However, due to the diverse nature of agent behaviour between the two models, extra routes were needed and were hence added in the GIS simulation to achieve more realistic evacuation pathways (Figure 20).

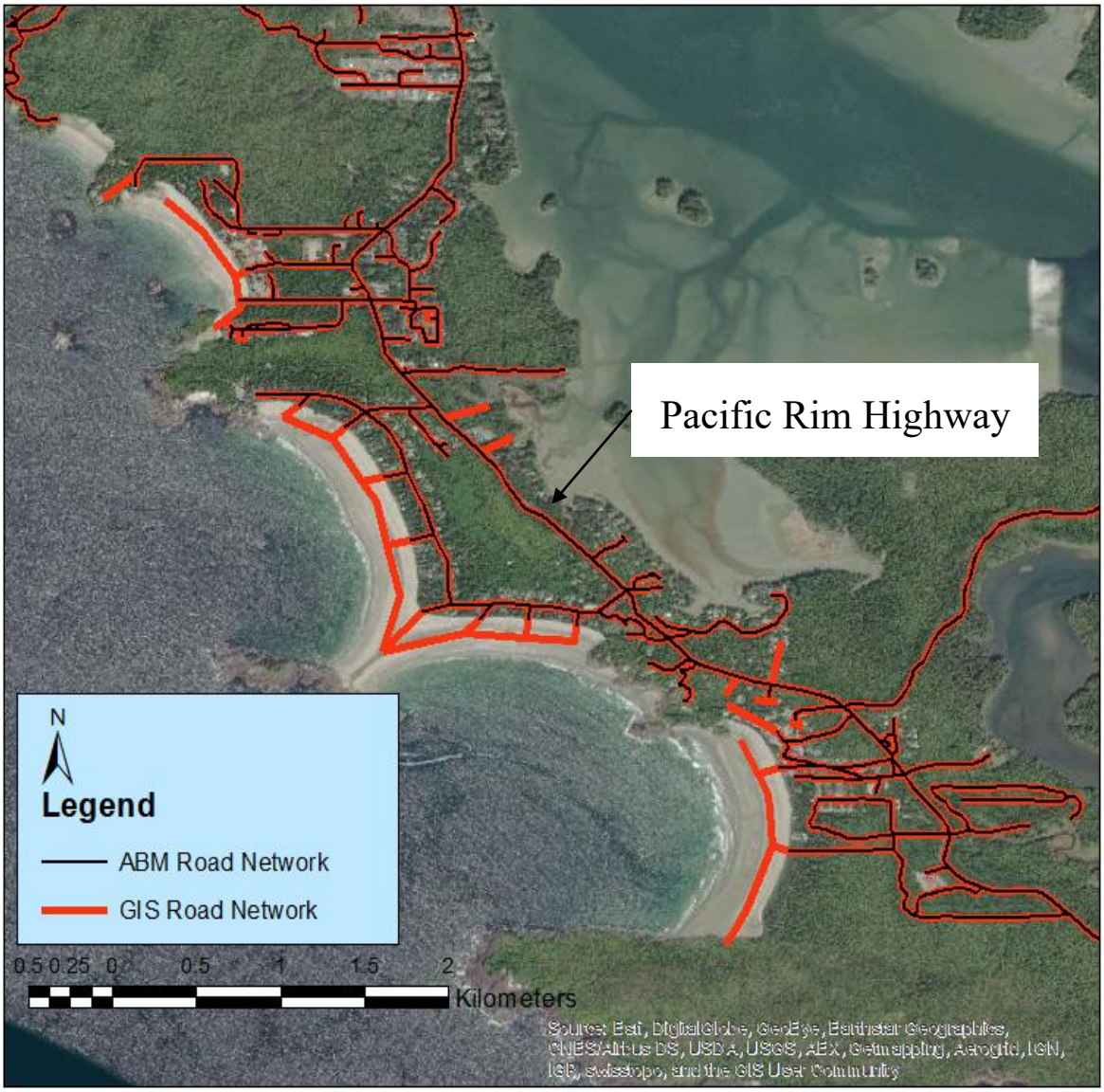

Figure 20: The black roads were used in the ABM as pathways for agents to traverse on. The ABM road network was then replicated into the GIS model, but additional roads were required due to nature of the agent behaviour. The road network used in GIS model is shown in red.

The additional extra routes are required as evacuees in the GIS model simulation cannot freely roam on the map without being on a pre-defined route. Evacuees in the GIS simulation first search for the closest road network and then get “snapped” to the route before starting their evacuation. This causes an underestimation of the time and distance travelled by an evacuee, especially for the beach areas where there are no pre-defined roads. Adding extra routes minimizes this effect by reducing the distance between an evacuee and a route to traverse on. The ABM does not have this limitation as agents can move freely on the map. Agents in the ABM start from their initial location and evacuate in a straight line to the nearest node in the road network, which accounts for the additional time needed to reach a road. Each link for the road network was also defined by their width so that the effect of crowd density on the evacuation speed could be accounted for in the ABM.

4.2.4 Evacuee Behaviour

While discussed in detail throughout this section, a summary of the ABM and GIS evacuee parameters are provided for reference in Table 4.

Table 4: Summary of the ABM agent and the GIS model evacuee parameters. A checkmark denotes its inclusion in the model while an X means that the parameter is not.

Model		Evacuee Classifications	Visitor		Local	
ABM	GIS	Age	0-64	65+	0-64	65+
✓	✓	Percent of Total Population	59.3% (SD), 58.3% (SN)	5.6% (SD), 5.5% (SN)	31.1%(SD), 32.0% (SN)	4.0% (SD), 4.2% (SN)
✓	✓	Evacuation Preparation Time	If on the beach or a residential house, agents start evacuating after 5 minutes. If in a resort building, agents start evacuating after 10 minutes. If it is a night-time scenario, all agents take 15 minutes to prepare for evacuation.			
✓	X	Casualty Estimation based on Depth Velocity Product (m2/s)	DV > 1.20	DV > 0	DV > 1.20	DV > 0
X	✓	Casualty Estimation based on available time after adjusting for evacuation preparation time and time of scenario (min)	44.33 (SD beach/house) 37.68 (SD resort) 15.51 (SN)	33.33 (SD beach/house) 28.33 (SD resort) 11.66 (SN)	44.33 (SD beach/house) 37.68 (SD resort) 15.51 (SN)	33.33 (SD beach/house) 28.33 (SD resort) 11.66 (SN)
✓	X	Default Walking Speed (m/s) Knoblauch (1996)	1.2	0.9	1.2	0.9
X	✓	Default Road Speed Limit (m/s)	0.9	0.9	0.9	0.9
✓	X	Walking Speed Variability due to Time of Scenario	For the SN case, all agents' walking speed is halved as navigation becomes more difficult due to lack of sufficient street lighting.			
X	✓	Available Time Variability due to Time of Scenario	For the SN case, all evacuees available time is halved as navigation becomes more difficult due to lack of sufficient street lighting.			
✓	X	Effect of Crowd Density	Walking speed is linearly reduced based on crowd density following Takabatake, Fujisawa et al. (2020).			
✓	X	Re-evacuation Behaviour	If an agent reaches an evacuation point that has reached max capacity, they will re-evacuate the second nearest evacuation point from their current location.			
✓	X	Evacuation Knowledge	As locals are familiar with the area and have been exposed to the town's tsunami preparedness efforts, they know to go to the closest evacuation point using the shortest path.		Only 50% of tourists are assumed to go to the nearest evacuation point, the other 50% go to the second closest evacuation point.	
X	✓	Evacuation Knowledge	All agents will always take the shortest path to the closest evacuation location.			
✓	X	Additional Agent Behaviour	Agents will not traverse in areas that have been flooded.			

4.2.4.1 Evacuee Demographics

When the initial location for each evacuee is being established, they are also classified as either a local or tourist. Then, their age range (i.e. 0-64, 65+) was assigned to each evacuee based on demographic data received by the local authorities of the District of Tofino. As a well-known and popular tourist destination, Tofino's tourists make up a significant portion of the community's demographic. For the Summer Daytime (SD) and Summer Night-Time (SN) scenarios, 64.9% and 63.8% of agents are considered tourists, respectively. Furthermore, tourist agents are assigned a 91.4% chance of being age 0-64, and an 8.6% chance of being of age 65+. Local agents have an 88.5% chance of being between 0-65, and an 11.5% chance of being 65+.

4.2.4.2 Evacuation Start Time

While there has been some focus on creating evacuation preparation time curves to probabilistically assign departure times to evacuees in an evacuation simulation, empirical data to support these curves is highly variable depending on the location and hazard event (Lindell & Prater, 2007; Takabatake et al., 2018). As no quantified data on the evacuation behaviour for the District of Tofino was available, assumptions were made in consultation with the emergency managers and constant evacuation preparation times were assigned. For both models, the preparation time needed for an evacuee to start evacuating was related to the initial location of the evacuee. Namely, if on the beach or a small residential house, evacuees start evacuating 5 minutes after the tsunami warning was sounded. If in a resort building, evacuees start evacuating after 10 minutes. In the case of the night-time scenario, all evacuees were assumed to take 15 minutes to prepare for evacuation.

4.2.4.3 Casualty Estimation

Two different methods for casualty estimation were employed. Cox et al. (2010) proposed a stability criteria to estimate when an evacuee should be considered a casualty when exposed to flooding. It was found that a depth-velocity (*DV*) product of more than 1.20 m^2/s causes evacuees to lose their stability and poses an extreme hazard for adults. Thus, evacuees under 65 years old were defined to become casualties once they experienced a *DV* of 1.20 m^2/s or more. If an elderly evacuee (i.e., 65+), experienced any type of flow (i.e. a *DV* greater than 0), they were considered to become a casualty. The *DV* product was directly calculated for each time step of the ABM from the M_w 9.0 tsunami hydrodynamic simulation results of Takabatake et al. (2020c). Depending on its location, each agent checks the *DV* product value of the mesh cell they are located in at each time step and, depending on its value, they are deemed casualties (or not).

For the GIS-based model, an evacuee's available time was used as the cost to determine whether they should be considered a casualty or not. As shown in Figure 21, Tofino's main road (Pacific Rim Highway) was found to be inundated approximately 2,300 s (38.33 min) after a M_w 9.0 CSZ earthquake occurs (Takabatake et al., 2020). Pacific Rim Highway (see Fig.3) was chosen as the ground marker for setting the tsunami arrival time as the instant when the highway is inundated translates into most of the land located close to the tidal flats on the western side of Tofino being inundated. Additionally, Pacific Rim Highway is the main road into Tofino that allows travel in the North-South direction and would be heavily used during evacuation (as seen in the ABM simulations) and hence cause potential major loss-of-life when inundated. Thus, an evacuee's baseline available evacuation time was set to 38.33 min (although the time was further adjusted to consider the required preparation time and moving speed of an evacuee). The use and adjustment of this available time is further discussed in detail in the proceeding section (4.2.4.4).

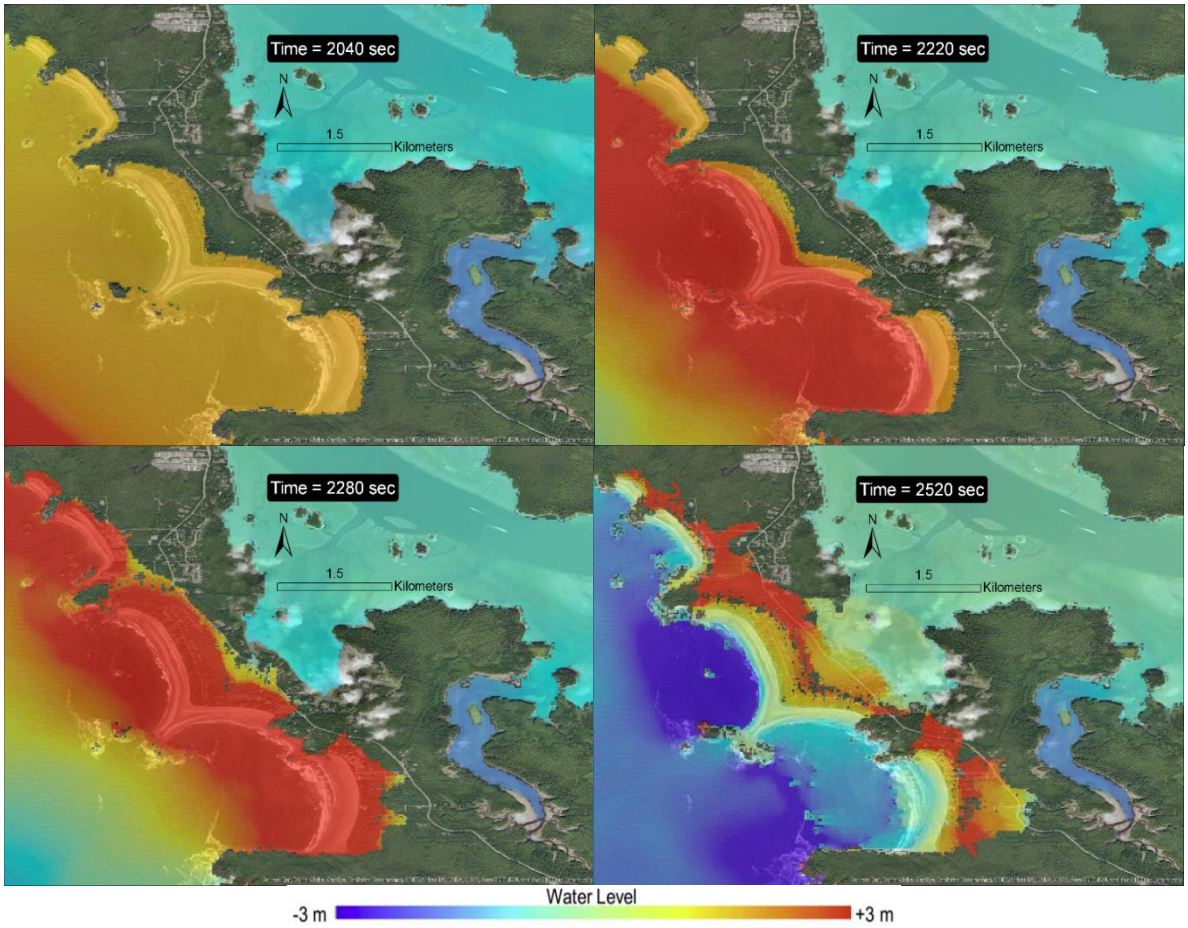

Figure 21: The propagation and inundation of the tsunami generated from a M_w 9.0 CSZ earthquake at 30, 34, 38, and 42 minutes after the earthquake occurrence. Around 2300s (38.33 min), the majority of the area around Tofino is inundated.

4.2.4.4 Moving Speed of Evacuees

The age of the ABM evacuees was used to define their pedestrian evacuation speed based on Knoblauch et al. (1996), who suggested design walking speeds of 1.2 m/s for those under the age of 65, and 0.9 m/s for those over the age of 65.

As evacuees congregate on to the roads to start their evacuation, their walking speed can be severely affected by the number of people surrounding them (Kim et al., 2019; Takabatake, et al., 2020) For the ABM, the crowd density (ρ) around an evacuee is defined by counting the number of other evacuees around him/her within a circle of a radius that is half of the road width with a maximum of 5 m at each time step. The speed

evacuee linearly decreases based on the calculated ρ. The reduction in walking speed used in Takabatake et al. (2020b) was implemented in this study, where:

$$\rho < 0.5 : \ no\ adjustment\ to\ v_{walking}\ (m/s) \tag{4}$$

$$0.5 < \rho < 3 : v_{walking} = \frac{0.2 - v_{walking}}{2.5} * (\rho - 0.5) + v_{walking}\ (m/s) \tag{5}$$

$$\rho > 3 : v_{walking} = 0.2\ (m/s) \tag{6}$$

The evacuees' speeds were also adjusted based on the scenario (daytime *vs* night-time). A field visit in March of 2019 conducted by Takabatake et al. (2020c) found that the minimal street lighting present in Tofino leads to very low visibility during the night. As this can severely impact the evacuation speed, all agents' evacuation speed was reduced (conservatively halved) for the night-time (SN) scenario.

In the GIS simulation, incorporating the differences in evacuees' speed as a function of their age is not possible. However, it is possible to set the travelling speed over a road section and the amount of time that each evacuee can travel for. This allows the user to vary an evacuee's evacuation potential in the form of the maximum distance that evacuees can travel with available time through the basic kinematic equation:

$$d_{evacuee} = v_{evacuee} * t_{available} \tag{7}$$

where $d_{evacuee}$ is the distance that an evacuee can travel based on the speed limit of the road, $v_{evacuee}$, and the time available for evacuation, $t_{available}$. This approach differs from the ABM methodology where agents have different speeds depending on their age and the crowd density, and also have a dynamic $t_{available}$ due to the more complex casualty estimation criterion when compared to the GIS simulation (section 4.2.4.3). Instead, evacuees in the GIS model were assumed to have a constant $v_{evacuee}$ of 0.9 m/s (the moving speed of a 65+ agent during the SD scenario) based on the speed

limit of the road, and the $t_{available}$ was adjusted to represent the varying moving speeds available in the ABM. For example, a 65+ evacuee travels at 0.9 m/s and can evacuate until the tsunami's first wave arrival at 38.33 minutes. After accounting for the evacuation preparation time (e.g., 5 minutes for an agent outside in the SD scenario), the evacuee effectively covers 1800 m after traveling for 33.33 minutes. Since a 0-64 evacuee can travel 1.33 times faster in the ABM (1.2 m/s instead of 0.9 m/s), the available time is increased by 1.33 times in the GIS model to reflect the effects of their faster moving speed. Thus, an evacuee aged 0 to 64 can evacuate in the GIS model for 44.33 minutes (i.e., 38.33 min minus the 5 minutes to prepare for evacuation, and then scaled by 1.33 times) allowing them to cover 2393 m even though their traveling speed is the same. The full list of available times used in the GIS model after adjusting for the evacuation preparation time and depending on the time of scenario is shown in Table 4. It should be noted that dynamically defining evacuation speed due to crowd density was not possible in the GIS model as the latter lacks the ability to implement time-based behaviours.

4.2.4.5 Route Choice

The District of Tofino regularly holds tsunami evacuation drills and provides exhaustive and user-friendly evacuation maps displayed throughout the community. Thus, it was assumed in the models that all local residents as well as the seasonal staff working in Tofino will evacuate to the closest evacuation location via the shortest route. On the other hand, tourists would most probably not possess the same level of evacuation knowledge as the locals but may find the closest evacuation location through the community hazard maps or through the guidance provided by locals during the evacuation. The ABM also assumes that 50% of tourists will chose the shortest route to closest evacuation location, while the other 50% will evacuate to the second closest evacuation location. Shortest routes to the closest and second closest evacuation locations were calculated using the A* algorithm (Anguelov, 2011) and relayed to each evacuee at each node on the road network. Once an evacuee successfully reaches an

evacuation location, they will first check if the maximum capacity has been reached (the capacities of each evacuation location were provided by the District of Tofino, and will be detailed in Section 2.5). If the capacity has not been reached, the evacuee is then considered to have successfully evacuated. Otherwise, the evacuee will resume its evacuation to the next closest evacuation location, omitting any previously visited locations. Evacuees are also prevented from crossing paths located on areas that have been inundated.

The varying levels of evacuation knowledge was not implemented in the GIS model simulation. Instead, each evacuee was defined to search for an evacuation location that can be reached within the available time. The *Network Analyst Tool* creates an Origin-Destination (OD) cost matrix to find the least-cost path while also considering the capacity of the evacuation location. As opposed to the ABM, since the GIS evacuees are all statically assigned an evacuation location at the start of the simulation, evacuees will never waste time evacuating to a location to only find it full (thus triggering a re-evacuation to the next closest evacuation location in the ABM). Instead, when using *Maximize Capacitated Coverage,* evacuees are assigned to a single evacuation location by solving an optimization problem where the number of evacuees is maximized around an evacuation location subject to capacity constraints.

4.2.5 Location and Capacity of Evacuation Areas

There are number of pre-existing locations that have been deemed evacuation locations (sometimes defined as assembly areas) as they are either outside of the inundation zone or are topographically elevated enough to avoid the tsunami-induced flooding. The geographical coordinates and capacities of each evacuation location was received from the local authorities of the District of Tofino and are shown in Figure 22.

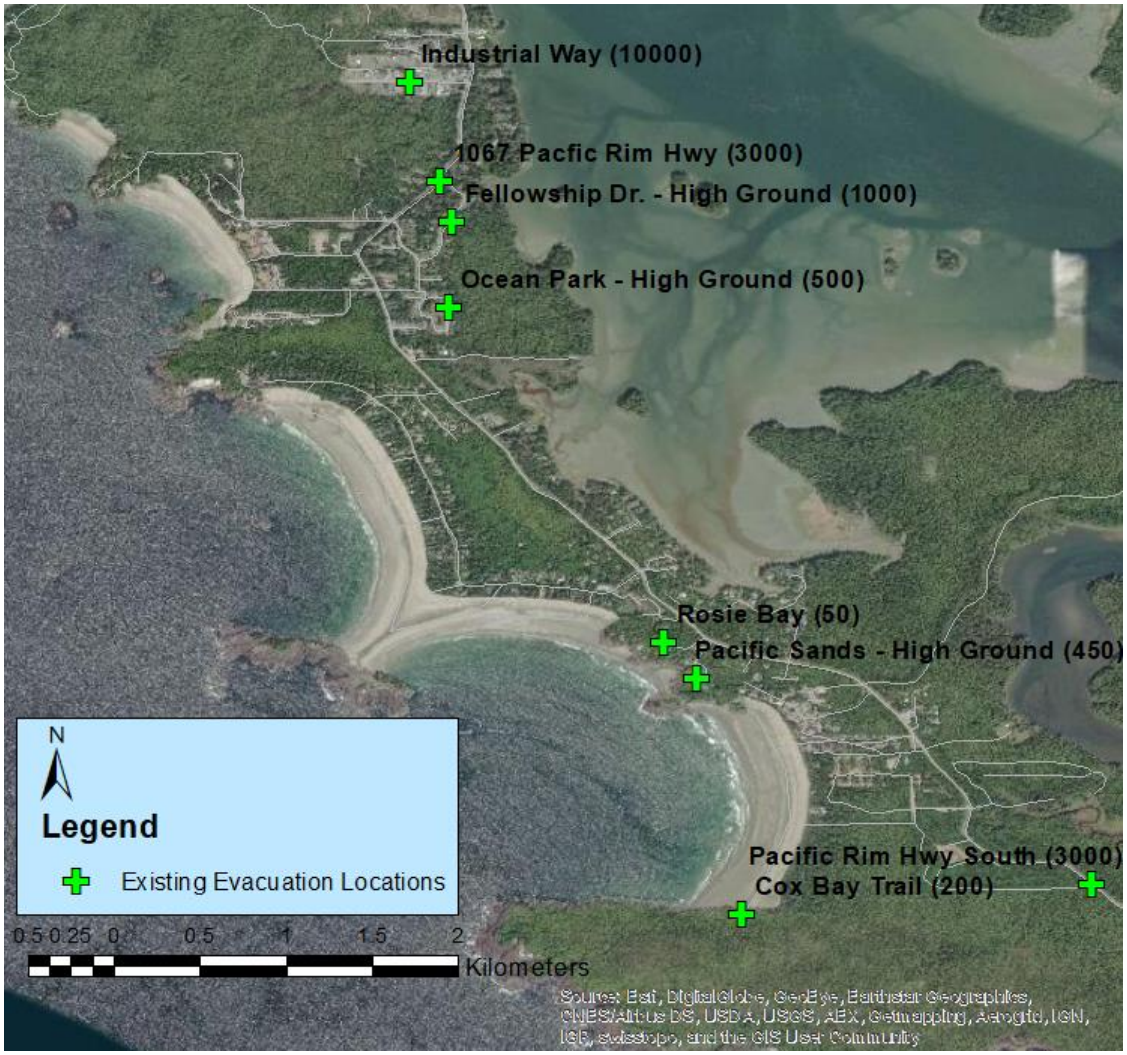

Figure 22: Existing evacuation locations used for the study; their capacity (in persons) is indicated in brackets.

To provide insight on the performance of the ABM and GIS models, several proposed candidate locations (shown in Figure 23) with unlimited capacity were also tested.

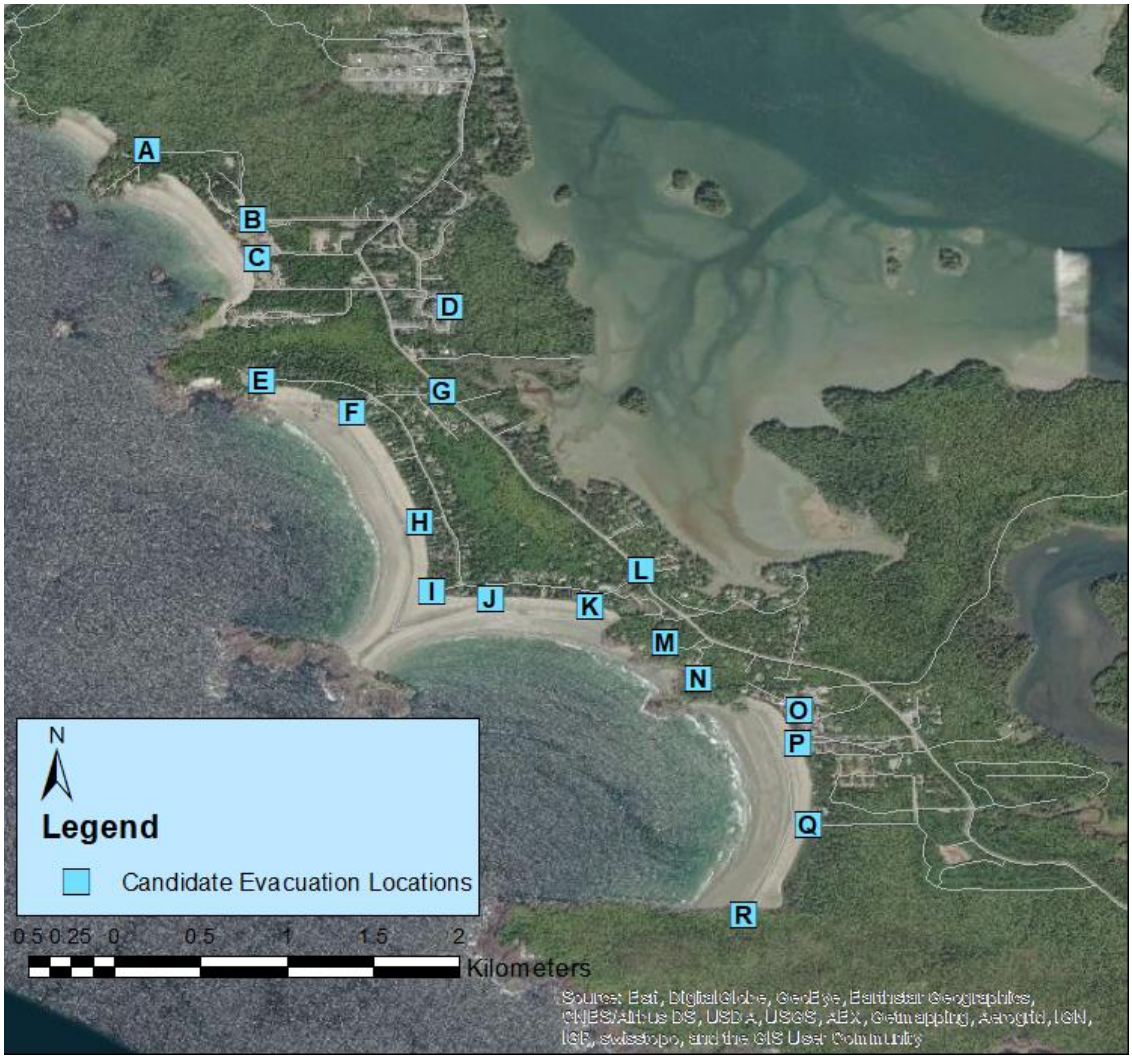

Figure 23: Candidate (proposed) evacuations used to assess the differences in results of the ABM and GIS simulations.

It should be noted that some of the proposed candidate evacuation locations (i.e. D, M, N and R) have the same geographical location as some of the existing ones. This is to test the performance of expanding an existing evacuation location as many pre-existing evacuation locations have relatively small capacities. The evacuation locations that did not reach full capacity during the baseline ABM test (i.e., only existing evacuation locations) were not added as candidate locations as they would not provide additional safety. This exercise has the added benefit of identifying the ideal geographic location for an additional evacuation location to minimize loss-of-life for Tofino, BC.

4.3 Results

4.3.1 Baseline Scenarios

There is an innate randomness to both the ABM and the GIS model due to the probabilistic approach of defining agent characteristics. This can lead to a spatial variance in the distribution of walking speeds, so a convergence study was performed whose results are shown in Figure 24.

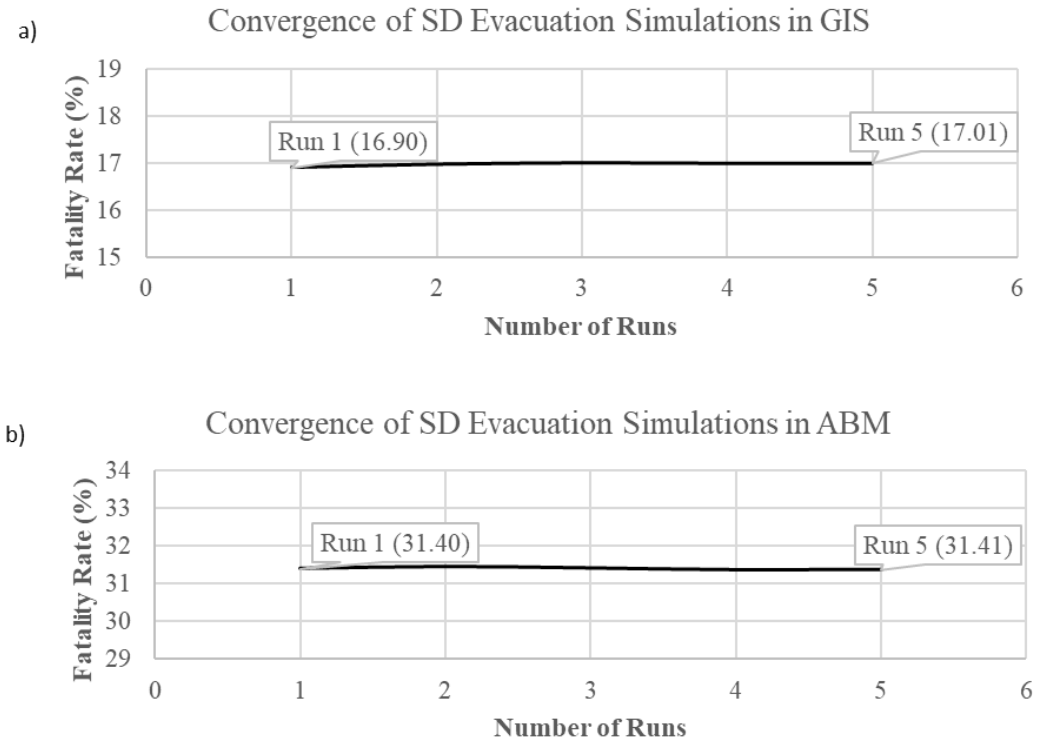

Figure 24: Convergence study for the GIS and ABM evacuation models. Five runs were performed for the SD scenario and the average fatality rate of runs performed is reported.

Similar results were reported in the convergence study performed by Takabatake et al. (2020c) (where they repeated their ABM 50 times)– there was minimal variance in fatality rates over the repeated simulations. Nevertheless, the ABM values reported in this study represent the average of three runs, and the GIS model values reported herein use the same population distribution that yielded the fatality rate that is closest to the average fatality rate found in the convergence study.

The SD and SN scenarios were first simulated as baseline scenarios with only the existing evacuation locations to examine the District of Tofino's present state of emergency preparedness. The ABM and GIS model evacuation simulations are compared with the results of Takabatake et al. (2020c) in Figure 25.

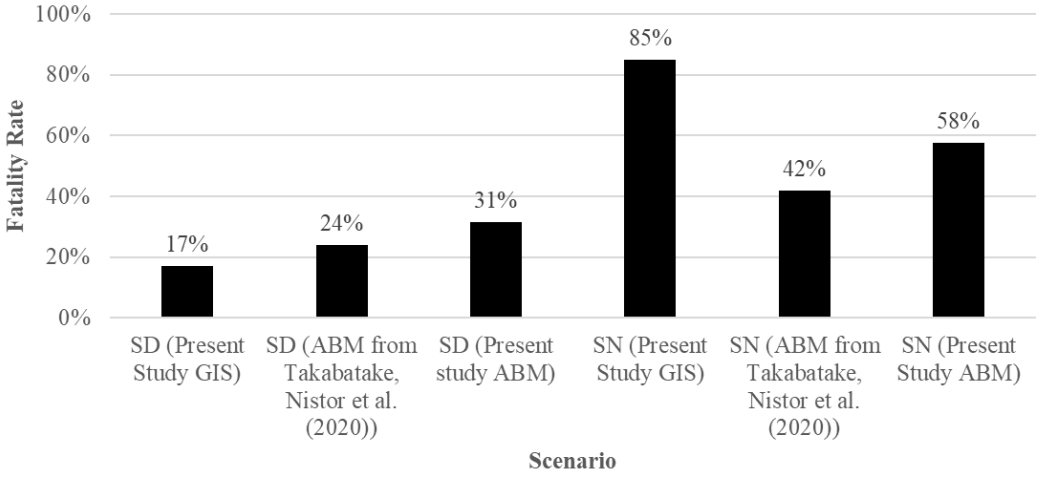

Figure 25: Comparison of the fatality rates found in the GIS and ABM evacuation simulations, and of the ABM simulation of Takabatake et al. (2020c).

The comparison between the present ABM results and those in Takabatake et al. (2020c) show that the inclusion of the effect of crowd density significantly increased the fatality rate for both the SD and SN scenarios by 29% and 38%, respectively. The higher increase in fatality rate in the SN scenario can be attributed to a higher concentration of people located in their homes compared to being spread out on the beaches in the SD scenario as seen in Figure 19. Namely, the effects of crowd density on moving speed, which were considered only in ABM, were more pronounced in the SN scenario.

For the SD scenario, the GIS-based evacuation model underpredicted the fatality rate by 45% when compared to this study's ABM. When comparing the initial location of agents that became casualties between ABM and GIS (Figure 26), there are similarities in the overall spatial distribution upon visual inspection for both the SD and SN

scenarios, but the magnitude of agents differs greatly.

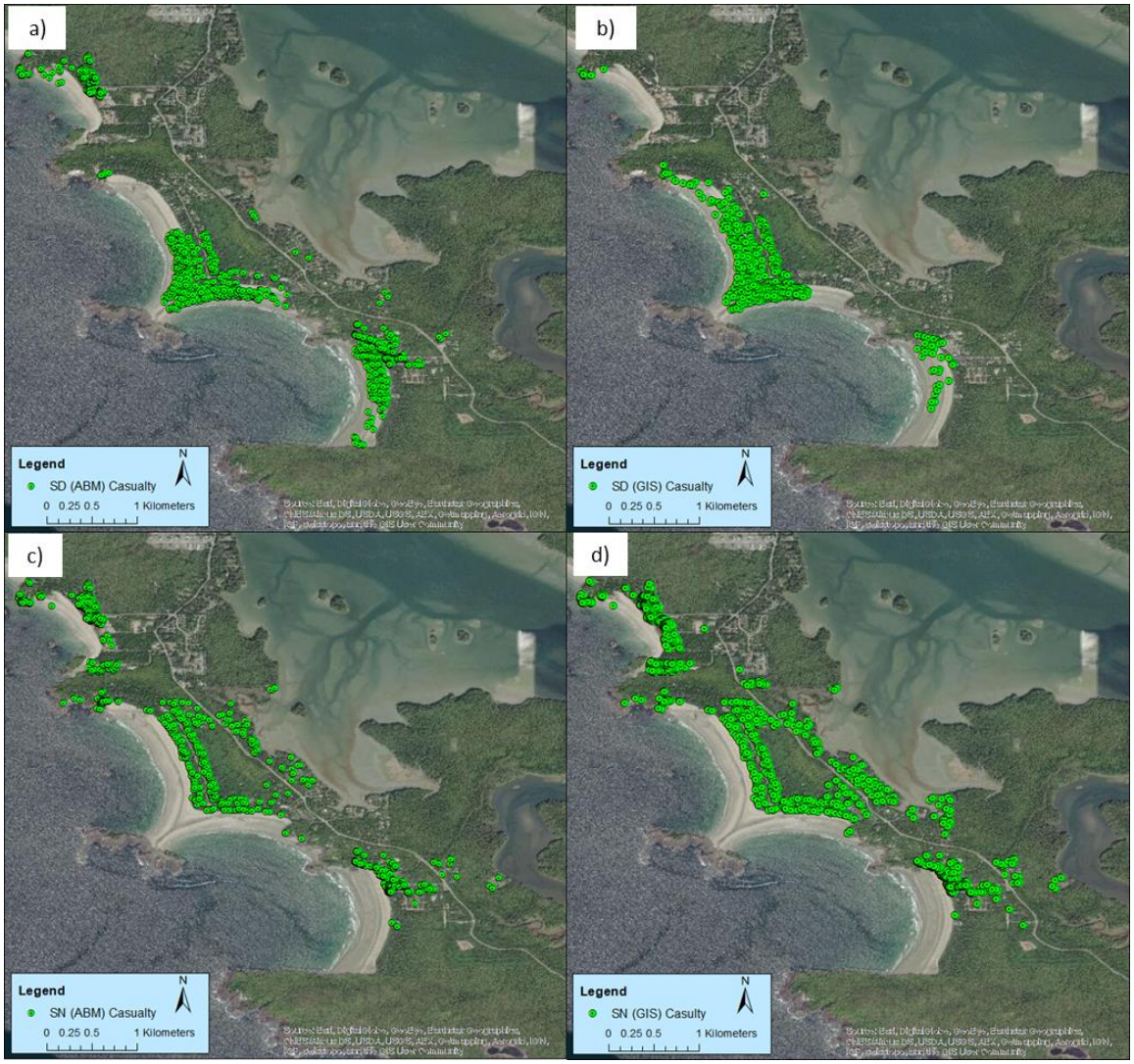

Figure 26: The initial location of the evacuees that became casualties during the tsunami evacuation for the following scenarios: a) SD (ABM) b) SD (GIS) c) SN (ABM) d) SN (GIS). All the scenarios presented consider the baseline scenario where only the existing evacuation locations are used during the simulation.

However, larger difference in the results can be found in the SD scenario. The ABM shows that many agents located on the southern beach, connected to Cox Bay Trail (see Figure 5), will not successfully evacuate unlike the GIS simulation. The source of this difference can be seen clearly in Figure 27, which shows a snapshot of the ABM evacuation.

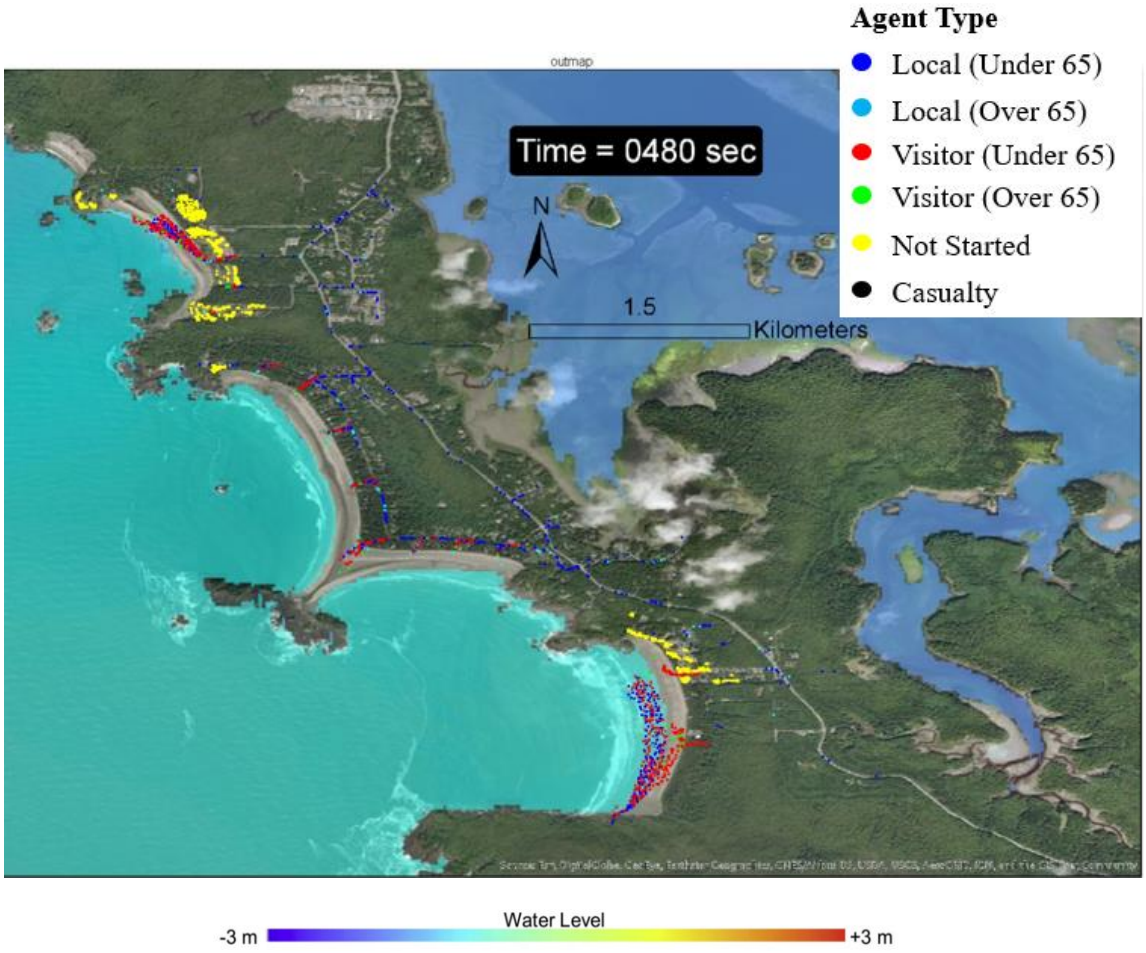

Figure 27: Snapshot of the evacuation in the ABM for the baseline SD scenario at 8 minutes after the earthquake event.

The southern beach is the first portion of Tofino that is inundated at approximately 8 minutes after the earthquake event. The agents evacuating to Cox Bay trail in the ABM became casualties at around 10 minutes after the earthquake event compared to the results of the GIS agents who are allowed to evacuate for their full available times indicated in Table 4. This underlines the importance of considering dynamic flooding

behaviour to properly estimate the number of casualties resulting from a tsunami event.

For the SN scenario, the GIS simulation produced a higher fatality rate by 47% than the ABM. This higher fatality rate is most likely attributed due to the relatively crude consideration of the reduced night-time walking speed: in the ABM simulation, agents have their walking speeds halved due to the lack of sufficient lighting. To account for this reduction in the evacuees walking speed in GIS, their available evacuation time was halved, leaving only twelve to sixteen minutes to reach a safe location. When examining the initial location of the agents who successfully evacuated (Figure 28), the largest difference in initial locations of successful evacuees for the SN scenario were found near two areas: near Rosie Bay and Pacific Sands – High Ground, and up north by Ocean Park – High Ground (see Figure 11c and 11d).

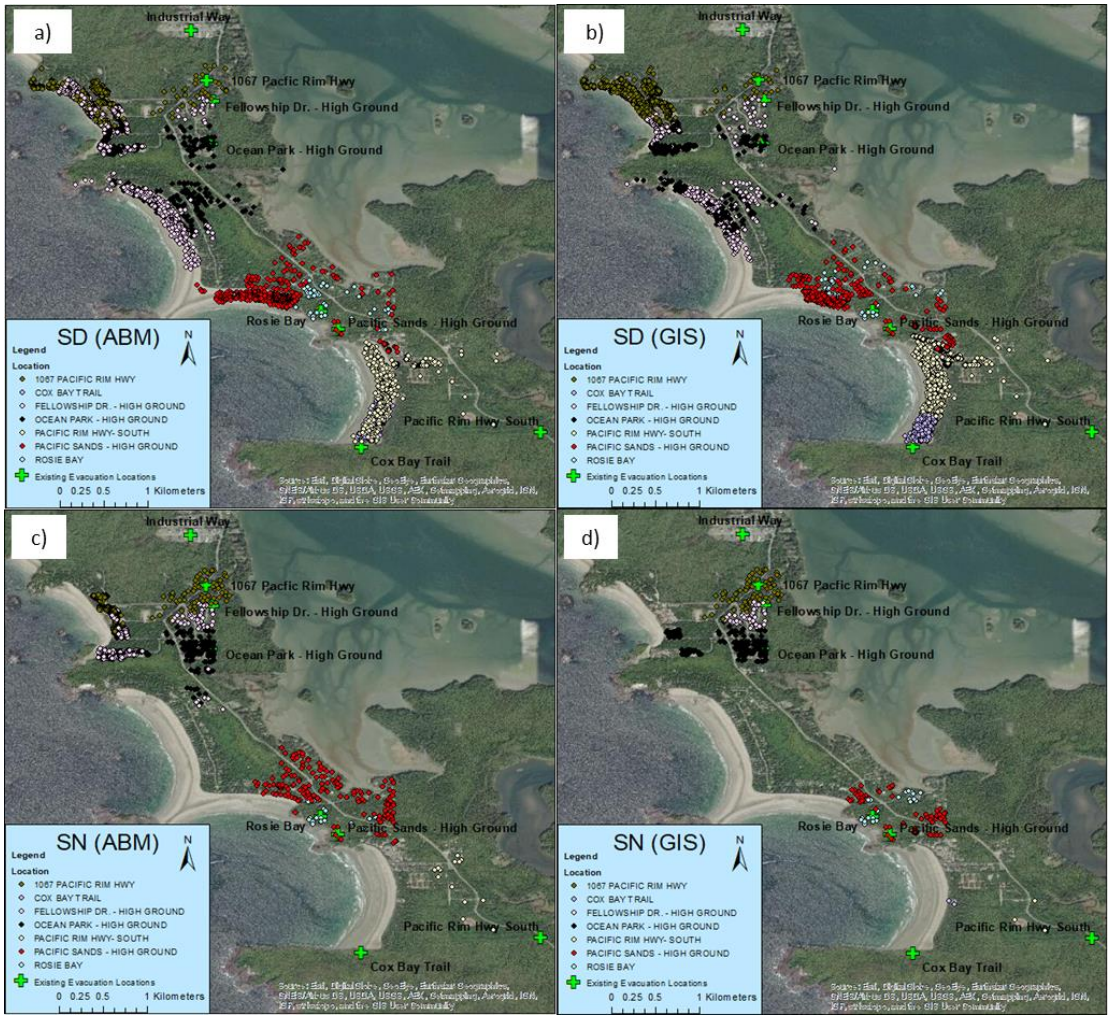

Figure 28: The initial location of successful evacuees is shown for the baseline a) SD (ABM) b) SD (GIS) c) SN (ABM) d) SN (GIS) scenarios. Each agent is coloured to reference which evacuation location they went to.

The tsunami inundation in Figure 21 shows that both those areas are not inundated due to their higher topography. In the GIS model, the evacuees are only considered safe if they reach an evacuation location during their allotted time. Since topographically, higher-located vertical evacuation sites can span large areas and not a single point, some evacuees may not be able to theoretically reach the evacuation location in their allotted time. However, they can be safe as long as they are in the zone where no inundation will occur. This reiterates the importance of incorporating the tsunami inundation results into the evacuation simulation, as it can consider such survivors (as shown in

the ABM results).

When examining the demand to capacity (D/C) ratios of the evacuation locations (shown in Figure 29), there was a strong correlation between the two modelling approaches for both the SD and the SN scenarios in terms of the ranking of the evacuation location usage. A direct comparison of the magnitude of the D/C ratios was not performed as the fatality rates between the GIS and ABM methodologies differ.

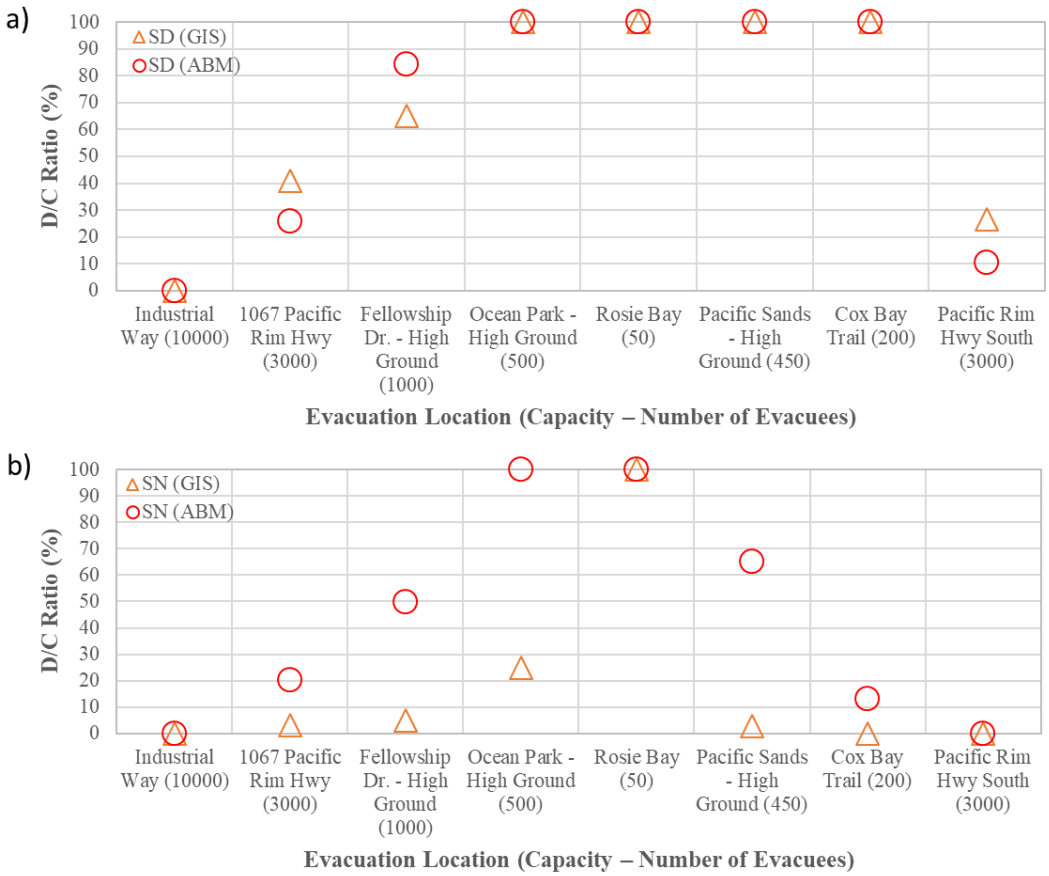

Figure 29: The demand capacity ratios of each existing evacuation location for a) the SD and b) the SN baseline scenarios in GIS and ABM. The evacuation locations are ordered spatially from North to South.

4.3.2 Additional Evacuation Locations

To show the effectiveness of the additional candidate evacuation locations in the ABM and GIS model simulation, Figure 30 shows the absolute decrease in fatality rate.

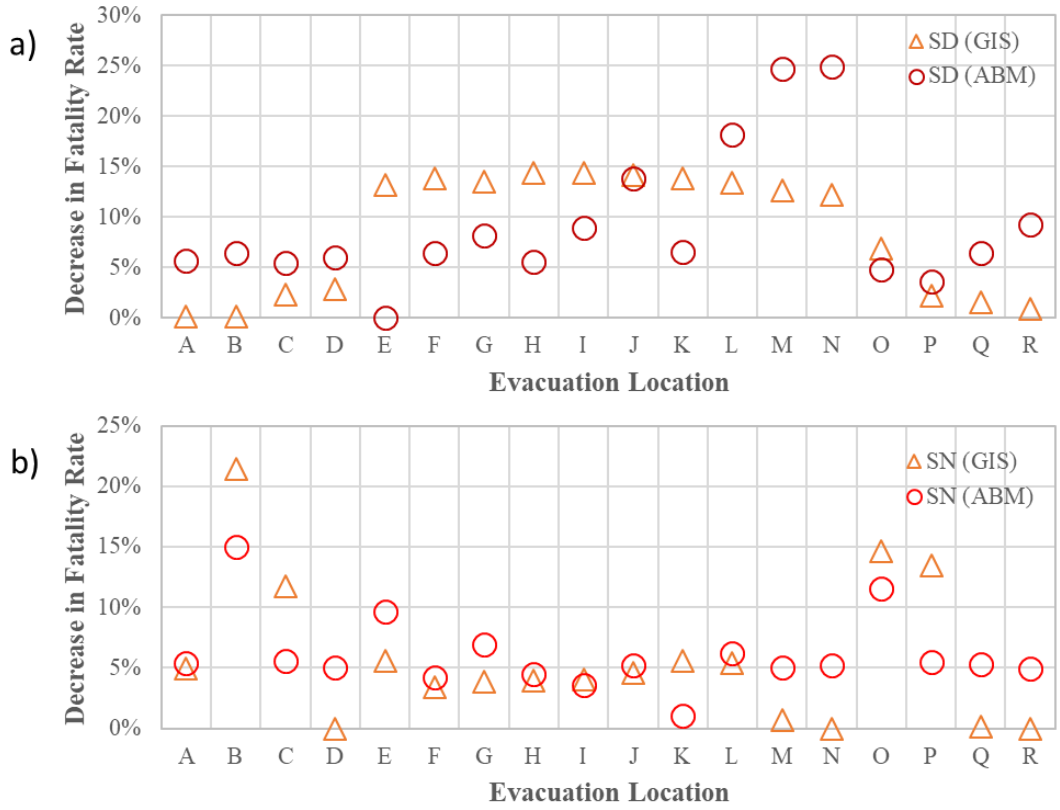

Figure 30: Decrease in fatality rate for the a) SD scenario and b) SN scenario from the baseline scenarios who only considers the existing evacuation locations.

In general, the centrally-located candidates (candidate locations are ordered from North to South along the west coast of the District of Tofino) performed better in both the GIS model and ABM simulations for the SD scenario. In the SN scenario, the opposite behaviour was observed—candidates on the north or south of the domain such as locations B and O were observed to reduce fatality rate more effectively. However, as drawing conclusions from absolute change in the fatality rate can be misleading due to the differences in the magnitude of the fatality rate between the two methodologies, the fatality rates when each candidate location is introduced are also compared in Figure 31.

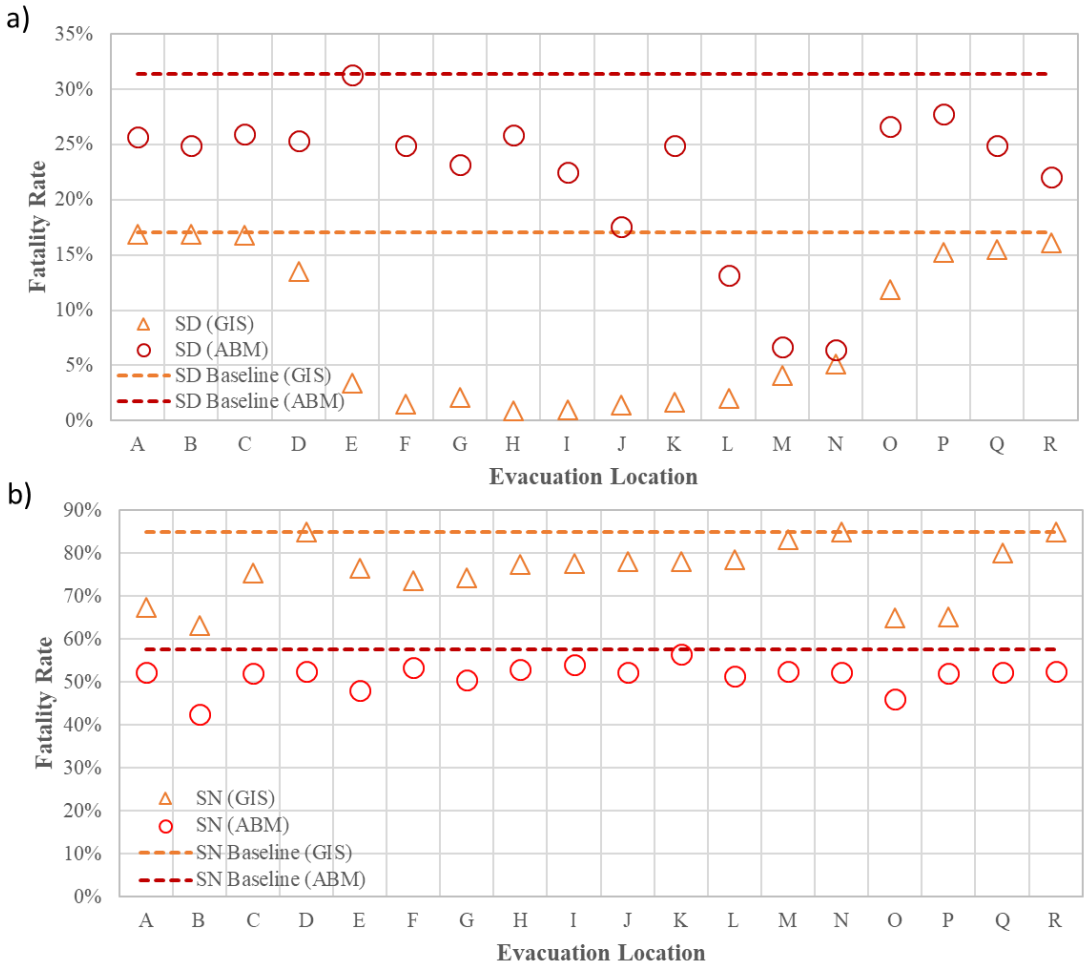

Figure 31: Fatality rates for the SD and SN scenario in GIS and ABM.

For the SD scenario, the central candidate locations decreased the fatality rate from the baseline of 31% for the ABM and 17% for the GIS model, similar to the trend seen when the absolute changes in the fatality rate were examined. For both models, expanding the Rosie Bay or Pacific Sands – High Ground (Candidates M and N) could potentially reduce fatality rates down to around 4 to 7 percent.

For the SN scenario, both simulations show that, while adding just a few additional evacuation locations such as Candidate B or O can reduce the fatality rate, no single location can significantly reduce the loss-of-life that may occur during a major tsunami event. Both models suggest that emergency preparedness plans should consider alternative methods such as additional zoning laws or extra evacuation routes to decrease fatality rates for SN scenarios.

4.4 Discussion

Agent behaviours such as the reduction in speed for night time scenarios, the level of evacuation knowledge for tourists and locals, and re-evacuating to another location when reaching a full evacuation location are all assumptions included based on engineering judgement due to the lack of studies focused on defining such human behaviour during tsunami evacuations. These assumptions may not perfectly portray a realistic picture of an agents' behaviour – for example when someone reaches an evacuation location deemed "full" (which is an estimated capacity by the local authorities of Tofino), there is a high potential that they will stay at that location and overcrowd it as they would be faced with an extreme hazard.

The limiting factor for the accuracy of agent-based models (ABMs) is not related to the availability of software or computational power. Rather than that, it is the lack of understanding and research on the human psychology and behaviour during tsunami evacuations. To obtain a better understanding of the behaviour which humans may exhibit during tsunami evacuation, surveys such as the ones performed after major tsunami events (e.g., Sun et al. (2013) for the 2011 Great East Japan Tsunami, Harnantyari et al. (2020) for the 2018 Palu Tsunami, Takabatake et al. (2019a) for the 2018 Sunda Strait Tsunami) should be conducted. However, it is still unclear how transferable the knowledge obtained from these surveys is between different locations, given the socio-economic and cultural conditions of each site may yield different levels of emergency preparedness and awareness. Thus, site-specific surveys may need to be conducted to model realistic evacuation behaviour of people for an area of interest. A full quantification of the evacuation behaviour is essential as evacuation models need to be realistically calibrated. Calibration is difficult due to the rare occurrence of tsunami events which make evacuation statistics difficult to collect. However, model validation may be possible through inter-model validation once the GIS model evacuation simulations reach further levels of complexity.

The introduction of using capacitated coverage models in commercial GIS programs has allowed users to access spatial analytical tools in a user-friendly manner. However, programs such as *ArcGIS* solve the capacitated coverage problem (Current and Storbeck, 1987) through heuristics, as computational time can be excessive to arrive at an exact solution as the number of locations, increase. Murray et al. (2019) compared the performance of commercial GIS products that use heuristics and Xpress (FICO, 2015) that can provide exact solutions to the maximum covering location problem (MCLP). They found that *ArcGIS* performed well in most cases, but approximately 50% of the test cases were not optimally solved. Xu et al. (2020) extended the work of Murray et al. (2019) by comparing the results of heuristic and exact solutions of the capacitated maximal covering location problem (CMCLP). They found that around 63% of their test scenarios did not find the optimal solutions using heuristics, with deviations in optimality of up to 10%. While the heuristic methods found in commercially-available GIS software (such as *ArcGIS)* allow an accessible user interface to set up and solve the CMCLP, the lack of technical documentation with respect to the heuristics used and options to adjust the heuristic parameters can be significant drawbacks when using commercial GIS software. Further studies using exact solutions to the CMCLP and the ABM can provide better insight on the differences in the two modelling methodologies.

For this study, a deterministic approach was employed when assessing the hazard by only utilizing the results of the M_w 9.0 CSZ earthquake. Probabilistic tsunami hazard assessments have already been conducted by other researchers for the CSZ (Park and Cox, 2016), and probabilistic evacuation assessments are possible through showing the different hazard zones for where agents are expected to become casualties under different earthquake scenarios. Other probabilistic approaches can also be implemented besides the source earthquake: tsunami surveys can provide distributions assigning the likelihood of a certain behaviour being exhibited during an evacuation. Through this,

different likelihoods of evacuation could be incorporated in evacuation models to provide insight on the evacuation risk through a probabilistic assessment.

For the GIS-based evacuation model, assigning a single available time for all the agents did not portray a realistic picture of the evacuation potential for the community. The use of multiple available times assigned to discretized zones as seen in Cheff et al. (2019) may provide a better estimate for the complex inundation process that the ABM can account for. Both the GIS and ABM simulations did not account for the effect of terrain slope on pedestrians which has been shown to have a significant effect by Wood and Schmidtlein (2013). They found that, accounting for slope and directionality of approach, changed the average pedestrian travel time by 30% when compared to a distance-only model such as the one used in this study. Additionally, the type of soil can negatively impact pedestrian walking speeds, especially for sandy environments (Schmidtlein and Wood, 2015), and should be taken into account in future studies.

4.5 Conclusions

The performance of two tsunami evacuation models, an ABM and a GIS model, was evaluated through a case study assessing the state of emergency preparedness for the District of Tofino, British Columbia, Canada, in combination with an investigation of potential emergency evacuation and mitigation options. The following conclusions were drawn:

- Both evacuation models show that the expansion of the Rosie Bay or Pacific Sands – High Ground evacuation areas significantly decreased the fatality rate to approximately 4 to 7% for the SD scenario.
- While the addition of extra evacuation locations for the SN scenario can decrease the fatality rate, it did not significantly mitigate the loss-of-life for either the GIS and ABM models.

- Other mitigation options (opening new evacuation routes, etc) should be investigated to mitigate loss-of-life in the SN scenario as this is the more critical scenario.

In terms of general observations on the differences in the performance of the ABM and GIS tsunami evacuation models, the following conclusions were drawn:

- The magnitude of fatality rate and facility demand for both models was significantly different.

- The GIS method used could not account for the dynamic flooding behaviour and agent interactions which were shown to have significant impact on the fatality rate.

- Both models showed comparable performance in the distribution of the initial location of successful evacuees, the evacuation location which the agents chose, and the D/C ratios.

- The GIS model, a simpler and faster tool, may provide insight on the overall trends of the evacuation potential, but should not be used when determining fatality rates, the demand of an evacuation location, or for creating safety zones without further development from their current state.

4.6 Acknowledgements

This work was funded through the University of Ottawa's Faculty of Engineering International Scholarship, by Ioan Nistor's NSERC Discovery Grant., and from the JSPS KAKENHI Grant Number JP1915104. The present work was performed as a part of activities of Research Institute of Sustainable Future Society, Waseda Research Institute for Science and Engineering, Waseda University. The authors would like to thank the District of Tofino and Northwest Hydraulics for their cooperation in acquiring data used in this study.

Chapter 5 Conclusions and Recommendations for Future Work

5.1 Conclusions

Two unique case studies were performed to better understand the coastal hazards that Canada experiences, which in turn, allows for more informed decision to be made when planning for flood resilient communities. The first case study was focused on the hydrodynamic modelling of storm surges in Canada's western Arctic and on the quality of the datasets that are used during the modelling process. In comparison to data acquired from proximate meteorological stations, the ERA5 reanalysis dataset provided an adequate description of atmospheric pressure, but did not accurately capture the peak wind speeds that occur during storm surge events. However, by prescribing high values for the wind drag coefficient, acceptable simulation results were attained. Non-traditional records of storm surges such as those from driftwood lines were found to significantly impact the expected return periods of storm surge events. The formulas presented by Joyce et al. (2019) to account for the presence of ice also saw good performance in the Beaufort Sea region.

In the second case study, the two evacuation models showed significantly different magnitudes when calculating mortality rates and demand for facilities, but showed similar trends. Both models agreed on a solution to reduce the loss-of-life for the community. While GIS may serve as a useful tool for initial investigation or as a validation tool for ABMs, ABMs are recommended for use when modelling evacuation until GIS methodologies are further developed.

5.2 Recommendations for Future Work

While both of the technical papers presented have offered their own unique discussions, conclusions, and recommendations in their appropriate sections, they were more focused on the scope of the individual paper. The suggestions in this section aim to tie these works to the broader domain of coastal engineering as a whole.

5.2.1 Hydrodynamic Hazard Modelling

- The quality of the ERA5 dataset was analyzed for only the western Arctic region of Canada. Due to its recent release, there is a lack of studies on ERA5's performance during stormy periods at other geographical locations where better sources of measurements are available and should be investigated.
- While the use of driftwood lines as high-water marks were examined in this study, the use of driftwood lines to calibrate inundation models by capturing the spatial distribution of the deposited driftwood line would be useful, especially for areas of limited data availability.
- An improvement on accounting for ice presence may be achieved by coupling the motion between ice and water, instead of only adjusting storm surge development from the presence of ice.
- There are countless guidelines issued by the provinces and territories of Canada which makes it difficult for engineers to ensure that they are following the most recent "best practices" available. The development of a guideline at the federal level may provide a uniform approach in planning for floods and draw on the expertise of practitioners across the entire country.
- Only a hazard assessment was performed as a part of this study. Probabilistic assessments can lend itself in evaluating risk to a community and add additional value-added products such as fragility curves.
- The impacts of climate change are thought to be most prominently visible in the Arctic regions. Future outlooks on storm surge hazards and risks under varying

climate scenarios would allow city planners to make more informed decisions.

5.2.2 Life Safety Assessments

- There is still a large uncertainty in modelling the behavior of evacuees during an extreme event. As experimental programs to observe evacuation behavior are logistically difficult, additional surveys can be collected to better understand evacuee behaviours.
- The validity of the survey results should also be examined if a large-scale evacuation experiment is performed to ensure the real-life behaviours are correctly reflected in the survey results.
- Evacuation planning is generally performed under a “worst-case” deterministic scenario. However, a life safety assessment that incorporates probabilistic hazards may provide useful information for city planners when determining areas of high risk.
- The ABM in this study was used to model tsunami evacuation. Other hydrodynamic hazards or natural disasters (e.g. storm surges, wildfires, volcano eruptions) may see benefit from the application of an ABM with similar properties to the one used in this study.

References

AECOM, 2013. Modelling of Potential Tsunami Inundation Limits and Run-up.

American Society of Civil Engineers, 2017. Minimum Design Loads and Associated Criteria for Buildings and Other Structures, 7th ed. American Society of Civil Engineers, Reston, VA. https://doi.org/10.1061/9780784414248

Anguelov, B., 2011. Video Game Pathfinding and Improvements to Discrete Search on Grid-based Maps (Master of Science). University of Pretoria, Pretoria.

Atkinson, D.E., 2005. Observed storminess patterns and trends in the circum-Arctic coastal regime. Geo-Mar Lett 25, 98–109. https://doi.org/10.1007/s00367-004-0191-0

Barnhart, K.R., Miller, C.R., Overeem, I., Kay, J.E., 2016. Mapping the future expansion of Arctic open water. Nature Clim Change 6, 280–285. https://doi.org/10.1038/nclimate2848

Birnbaum, G., Lüpkes, C., 2002. A new parameterization of surface drag in the marginal sea ice zone. Tellus A: Dynamic Meteorology and Oceanography 54, 107–123. https://doi.org/10.3402/tellusa.v54i1.12121

Booth, L., Quinn, F., 1995. TWENTY-FIVE YEARS OF THE CANADA WATER ACT. Canadian Water Resources Journal 20, 65–90. https://doi.org/10.4296/cwrj2002065

Borja, A., White, M.P., Berdalet, E., Bock, N., Eatock, C., Kristensen, P., Leonard, A., Lloret, J., Pahl, S., Parga, M., Prieto, J.V., Wuijts, S., Fleming, L.E., 2020. Moving Toward an Agenda on Ocean Health and Human Health in Europe. Front. Mar. Sci. 7, 37. https://doi.org/10.3389/fmars.2020.00037

Brodtkorb, P.A., Johannesson, P., Lindgren, G., Rychlik, I., Ryden, J., Sjo, E., 2000. WAFO - a Matlab toolbox for analysis of random waves and loads. Presented at the The Tenth International Offshore and Polar Engineering Conference, 28

May-2 June, Seattle, Washington, USA, International Society of Offshore and Polar Engineers, p. 8.

Brown, D.G., Riolo, R., Robinson, D.T., North, M., Rand, W., 2005. Spatial process and data models: Toward integration of agent-based models and GIS. J Geograph Syst 7, 25–47. https://doi.org/10.1007/s10109-005-0148-5

Bryant, K., Akbar, M., 2016. An Exploration of Wind Stress Calculation Techniques in Hurricane Storm Surge Modeling. JMSE 4, 58. https://doi.org/10.3390/jmse4030058

Burns, B.M., Service, C.A.E., 1973. The Climate of the Mackenzie Valley - Beaufort Sea, Climatological studies. Environment Canada, Atmospheric Environment.

Chapman, R., Kim, S.-C., Mark, D., 2009. Storm-Induced Water Level Prediction Study for the Western Coast of Alaska.

Cheff, I., Nistor, I., Palermo, D., 2019. Pedestrian evacuation modelling of a Canadian West Coast community from a near-field Tsunami event. Nat Hazards 98, 229–249. https://doi.org/10.1007/s11069-018-3487-5

Cherniawsky, J.Y., Titov, V.V., Wang, K., Li, J.-Y., 2007. Numerical Simulations of Tsunami Waves and Currents for Southern Vancouver Island from a Cascadia Megathrust Earthquake. Pure appl. geophys. 164, 465–492. https://doi.org/10.1007/s00024-006-0169-0

Chock, G., Robertson, I.N., Kriebel, D.L., Francis, M., Nistor, I., 2013. Tohoku, Japan, Earthquake and Tsunami of 2011: performance of structures under tsunami loads. American Society of Civil Engineers, Reston, Virginia.

Clague, J.J., 2002. The Earthquake Threat in Southwestern British Columbia: A Geologic Perspective. Natural Hazards 26, 28.

Clague, J.J., Bobrowsky, P.T., Hutchinson, I., 2000. A review of geological records of large tsunamis at Vancouver Island, British Columbia, and implications for hazard. Quaternary Science Reviews 19, 849–863. https://doi.org/10.1016/S0277-3791(99)00101-8

Cova, T.J., Church, R.L., 1997. Modelling community evacuation vulnerability using GIS. International Journal of Geographical Information Science 11, 763–784. https://doi.org/10.1080/136588197242077

Cox, R.J., Shand, T.D., Blacka, M.J., 2010. Australian Rainfall and Runoff Revision Projects - Project 10: Appropriate Safety Criteria for People.

Current, J.R., Storbeck, J.E., 1987. Capacitated covering models.

Danard, M.B., Rasmussen, M.C., Murty, T.S., Henry, R.F., Kowalik, Z., Venkatesh, S., 1989. Inclusion of ice cover in a storm surge model for the Beaufort Sea. Nat Hazards 2, 153–171. https://doi.org/10.1007/BF00141389

Dengler, L., 1998. Strategic Implmentation Plan for Tsunami Mitigation Projects, approved by the Mitigation Subcommittee of the National Tsunai Hazard Mitigation Program. NOAA/Pacific Marine Environmental Laboratory, Technical Report NOAA Tech. Memo. ERL PMEL-113 (PB99-115552).

Department of Public Works, 1971. Investigation of storm, September 13-16, 1970 - Mackenzie Delta Region, Beaufort Sea. Unpublished technical report by Public Works of Canada.

Dullaart, J.C.M., Muis, S., Bloemendaal, N., Aerts, J.C.J.H., 2020. Advancing global storm surge modelling using the new ERA5 climate reanalysis. Clim Dyn 54, 1007–1021. https://doi.org/10.1007/s00382-019-05044-0

Fetterer, F., Knowles, K., Savoie, M., Windnagel, A.K., 2017. Sea Ice Index, in: NSIDC: National Snow and Ice Data Center. Boulder, Colarado, USA. https://doi.org/10.7265/N5K072F8

FICO, 2015. Xpress. Fair Isaac Corp.

Flather, R.A., 1976. Results from a storm surge prediction model of the north-west European continental shelf for April, November and December 1973.

Folke, C., Carpenter, S., Elmqvist, T., Gunderson, L., Holling, C., Walker, B., 2002. Resilience and Sustainable Development: Building Adaptive Capacity in a World of Transformations 31, 4.

Ford, J.D., Couture, N., Bell, T., Clark, D.G., 2018. Climate change and Canada's north coast: research trends, progress, and future directions. Environ. Rev. 26, 82–92. https://doi.org/10.1139/er-2017-0027

Foreman, M.G.G., Cherniawsky, J.Y., Ballantyne, V.A., 2009. Versatile Harmonic Tidal Analysis: Improvements and Applications. Journal of Atmospheric and Oceanic Technology 26, 806–817. https://doi.org/10.1175/2008JTECHO615.1

Government of Canada, P.S.C., 2018. Canadian Disaster Database [WWW Document]. URL https://cdd.publicsafety.gc.ca/srchpg-eng.aspx?dynamic=false (accessed 8.23.20).

Graham, R.M., Hudson, S.R., Maturilli, M., 2019. Improved Performance of ERA5 in Arctic Gateway Relative to Four Global Atmospheric Reanalyses. Geophysical Research Letters 46, 6138–6147. https://doi.org/10.1029/2019GL082781

Harnantyari, A.S., Takabatake, T., Esteban, M., Valenzuela, P., Nishida, Y., Shibayama, T., Achiari, H., Rusli, Marzuki, A.G., Marzuki, M.F.H., Aránguiz, R., Kyaw, T.O., 2020. Tsunami awareness and evacuation behaviour during the 2018 Sulawesi Earthquake tsunami. International Journal of Disaster Risk Reduction 43, 101389. https://doi.org/10.1016/j.ijdrr.2019.101389

Harper, J.R., Henry, R.F., Stewart, G.G., 1988. Maximum Storm Surge Elevations in the Tuktoyaktuk Region of the Canadian Beaufort Sea. ARCTIC 41, 48–52. https://doi.org/10.14430/arctic1691

Henry, R.F., 1975. Storm Surges.

Henry, R.F., 1974. Storm Surges in the Southern Beaufort Sea.

Henry, R.F., Heaps, N.S., 1976. Storm Surges in the Southern Beaufort Sea. Journal of the Fisheries Research Board of Canada 2362–2376.

Hersbach, H., Bell, B., Berrisford, P., Hirahara, S., Horányi, A., Muñoz-Sabater, J., Nicolas, J., Peubey, C., Radu, R., Schepers, D., Simmons, A., Soci, C., Abdalla, S., Abellan, X., Balsamo, G., Bechtold, P., Biavati, G., Bidlot, J.,

Bonavita, M., Chiara, G.D., Dahlgren, P., Dee, D., Diamantakis, M., Dragani, R., Flemming, J., Forbes, R., Fuentes, M., Geer, A., Haimberger, L., Healy, S., Hogan, R.J., Hólm, E., Janisková, M., Keeley, S., Laloyaux, P., Lopez, P., Lupu, C., Radnoti, G., Rosnay, P. de, Rozum, I., Vamborg, F., Villaume, S., Thépaut, J.-N., 2020. The ERA5 global reanalysis. Quarterly Journal of the Royal Meteorological Society 146, 1999–2049. https://doi.org/10.1002/qj.3803

Hervouet, J., Ata, R., 2019. User manual of opensource software TELEMAC-2D. EDF-R&D.

Holling, C.S., 1973. Resilience and Stability of Ecological Systems. Annu. Rev. Ecol. Syst. 4, 1–23. https://doi.org/10.1146/annurev.es.04.110173.000245

Hoque, Md.A., Perrie, W., Solomon, S.M., 2017. Evaluation of two spectral wave models for wave hindcasting in the Mackenzie Delta. Applied Ocean Research 62, 169–180. https://doi.org/10.1016/j.apor.2016.11.009

Hwacha, V., 2005. CANADA'S EXPERIENCE IN DEVELOPING A NATIONAL DISASTER MITIGATION STRATEGY: A DELIBERATIVE DIALOGUE APPROACH. Mitigation and Adaptation Strategies for Global Change 10, 17.

Imamura, F., 1997. Numerical Method of Tsunami Simulation with the Leap-Frog Scheme.

International Hydrographic Organization, 2019. Gridded bathymetry data (General Bathymetric Chart of the Oceans). [WWW Document]. GEBCO. URL https://www.gebco.net/data_and_products/gridded_bathymetry_data/ (accessed 8.24.20).

James, T.S., Henton, J.A., Leonard, L.J., Darlington, A., Forbes, D.L., Craymer, M., 2015. Tabulated values of relative sea-level projections in Canada and the adjacent mainland United States (No. 7942). https://doi.org/10.4095/297048

Japan Meteorological Agency, 2013. JRA-55: Japanese 55-year Reanalysis, Daily 3-Hourly and 6-Hourly Data. https://doi.org/10.5065/D6HH6H41

Johnson, H.K., HøJjstrup, J., 1998. On the Dependence of Sea Surface Roughness on Wind Waves. JOURNAL OF PHYSICAL OCEANOGRAPHY 28, 15.

Johnstone, W.M., Lence, B.J., 2012. Use of Flood, Loss, and Evacuation Models to Assess Exposure and Improve a Community Tsunami Response Plan: Vancouver Island. Nat. Hazards Rev. 13, 162–171. https://doi.org/10.1061/(ASCE)NH.1527-6996.0000056

Jonientz-Trisler, C., Simmons, R.S., Yanagi, B.S., Crawford, G.L., Darienzo, M., Eisner, R.K., Petty, E., Priest, G.R., 2004. Planning for Tsunami-Resilient Communities. Natural Hazards 35, 121–139.

Joyce, B.R., Pringle, W.J., Wirasaet, D., Westerink, J.J., Van der Westhuysen, A.J., Grumbine, R., Feyen, J., 2019. High resolution modeling of western Alaskan tides and storm surge under varying sea ice conditions. Ocean Modelling 141, 101421. https://doi.org/10.1016/j.ocemod.2019.101421

Jumadi, Carver, S., Quincey, D., 2016. A Conceptual Framework of Volcanic Evacuation Simulation of Merapi Using Agent-based Model and GIS. Procedia - Social and Behavioral Sciences 227, 402–409. https://doi.org/10.1016/j.sbspro.2016.06.092

Katada, T., Kuwasawa, N., Yeh, H., Pancake, C., 2006. INTEGRATED SIMULATION OF TSUNAMI HAZARDS. Presented at the 100th Anniversary Earthquake Conference including the 8th U.S National Conference on Earthquake Engineering (8NCEE), the SSA Centennial Meeting, and the OES Disaster Resistant California Conference, p. 8.

Kim, H., Han, J., Han, S., 2019. Analysis of evacuation simulation considering crowd density and the effect of a fallen person. J Ambient Intell Human Comput 10, 4869–4879. https://doi.org/10.1007/s12652-019-01184-7

Knoblauch, R.L., Pietrucha, M.T., Nitzburg, M., 1996. Field Studies of Pedestrian Walking Speed and Start-Up Time. Transportation Research Record 1538, 37–38. https://doi.org/10.3141/1538-04

Kowalik, Z., 1984. Storm surges in the Beaufort and Chukchi Seas. J. Geophys. Res. 89, 10570. https://doi.org/10.1029/JC089iC06p10570

Kundzewicz, Z.W., Kanae, S., Seneviratne, S.I., Handmer, J., Nicholls, N., Peduzzi, P., Mechler, R., Bouwer, L.M., Arnell, N., Mach, K., Muir-Wood, R., Brakenridge, G.R., Kron, W., Benito, G., Honda, Y., Takahashi, K., Sherstyukov, B., 2014. Flood risk and climate change: global and regional perspectives. Hydrological Sciences Journal 59, 1–28. https://doi.org/10.1080/02626667.2013.857411

Laghi, M., Cavalletti, A., Polo, P., 2006. EVACUATION ROUTES TOOLS ArcGIS® toolbox.

Lemmen, D.S., Warren, F.J., James, T.S., Clarke, C.S.L.M., 2016. Canada's marine coasts in a changing climate. Natural Resources Canada.

Leonard, L.J., Rogers, G.C., Mazzotti, S., 2014. Tsunami hazard assessment of Canada. Nat Hazards 70, 237–274. https://doi.org/10.1007/s11069-013-0809-5

Lindell, M.K., Prater, C.S., 2007. Critical Behavioral Assumptions in Evacuation Time Estimate Analysis for Private Vehicles: Examples from Hurricane Research and Planning. J. Urban Plann. Dev. 133, 18–29. https://doi.org/10.1061/(ASCE)0733-9488(2007)133:1(18)

Liu, H., Silva, E.A., Wang, Q., 2016. Incorporating GIS data into an agent-based model to support planning policy making for the development of creative industries. J Geogr Syst 18, 205–228. https://doi.org/10.1007/s10109-016-0229-7

Lüpkes, C., Gryanik, V.M., Hartmann, J., Andreas, E.L., 2012. A parametrization, based on sea ice morphology, of the neutral atmospheric drag coefficients for weather prediction and climate models. Journal of Geophysical Research: Atmospheres 117. https://doi.org/10.1029/2012JD017630

Manson, G.K., 2005. ON THE COASTAL POPULATIONS OF CANADA AND THE WORLD. Presented at the Canadian Coastal Conference, p. 11.

Manson, G.K., Solomon, S.M., 2007. Past and future forcing of Beaufort Sea coastal change. Atmosphere-Ocean 45, 107–122. https://doi.org/10.3137/ao.450204

Mas, E., Koshimura, S., Imamura, F., Suppasri, A., Muhari, A., Adriano, B., 2015. Recent Advances in Agent-Based Tsunami Evacuation Simulations: Case Studies in Indonesia, Thailand, Japan and Peru. Pure Appl. Geophys. 172, 3409–3424. https://doi.org/10.1007/s00024-015-1105-y

MMM Group Limited, 2014. National Floodplan Management Framework.

Moudrak, N., Feltmate, D.B., 2019. Ahead of the Storm - Developing Flood-Resilience Guidance for Canada's Commercial Real Estate.

Muis, S., Apecechea, M.I., Dullaart, J., de Lima Rego, J., Madsen, K.S., Su, J., Yan, K., Verlaan, M., 2020. A High-Resolution Global Dataset of Extreme Sea Levels, Tides, and Storm Surges, Including Future Projections. Front. Mar. Sci. 7, 263. https://doi.org/10.3389/fmars.2020.00263

Murray, A.T., Xu, J., Wang, Z., Church, R.L., 2019. Commercial GIS location analytics: capabilities and performance. International Journal of Geographical Information Science 33, 1106–1130. https://doi.org/10.1080/13658816.2019.1572898

Murty, T.S., Polavarapu, R.J., 1979. Influence of an ice layer on the propagation of long waves. Marine Geodesy 2, 99–125. https://doi.org/10.1080/15210607909379342

Okada, Y., 1985. Surface deformation due to shear and tensile faults in a half-space. Bull. Seismol. Soc. Am 75, 1135–1154.

Palermo, D., Nistor, I., Saatcioglu, M., Ghobarah, A., 2013. Impact and damage to structures during the 27 February 2010 Chile tsunami. Can. J. Civ. Eng. 40, 750–758. https://doi.org/10.1139/cjce-2012-0553

Park, H., Cox, D.T., 2016. Probabilistic assessment of near-field tsunami hazards: Inundation depth, velocity, momentum flux, arrival time, and duration applied

to Seaside, Oregon. Coastal Engineering 117, 79–96. https://doi.org/10.1016/j.coastaleng.2016.07.011

Public Safety Canada, 2018a. Canada's Platform for Disaster Risk Reduction [WWW Document]. Canada's Platform for Disaster Risk Reduction. URL https://www.publicsafety.gc.ca/cnt/mrgnc-mngmnt/dsstr-prvntn-mtgtn/pltfrm-dsstr-rsk-rdctn/index-en.aspx (accessed 8.23.20).

Public Safety Canada, 2018b. Federal Flood Mapping Guidelines Series [WWW Document]. Federal Flood Mapping Guideline Series. URL https://www.publicsafety.gc.ca/cnt/mrgnc-mngmnt/dsstr-prvntn-mtgtn/ndmp/fldpln-mppng-en.aspx (accessed 8.23.20).

Public Safety Canada, 2008. Canada's National Disaster Mitigation Strategy.

Quinn, F., 1985. The Evolution of Federal Water Policy. Canadian Water Resources Journal 10, 21–33. https://doi.org/10.4296/cwrj1004021

Ramon, J., Lledó, L., Torralba, V., Soret, A., Doblas-Reyes, F.J., 2019. What global reanalysis best represents near-surface winds? Quarterly Journal of the Royal Meteorological Society 145, 3236–3251. https://doi.org/10.1002/qj.3616

Reimnitz, E., Maurer, D.K., 1979. Effects of Storm Surges on the Beaufort Sea Coast, Northern Alaska. ARCTIC 32, 329–344. https://doi.org/10.14430/arctic2631

Richardson, G.R.A., Canada, Natural Resources Canada, 2010. Adapting to climate change: an introduction for Canadian municipalities. Natural Resources Canada, Ottawa.

Ruangrassamee, A., Yanagisawa, H., Foytong, P., Lukkunaprasit, P., Koshimura, S., Imamura, F., 2006. Investigation of Tsunami-Induced Damage and Fragility of Buildings in Thailand after the December 2004 Indian Ocean Tsunami. Earthquake Spectra 22, 377–401. https://doi.org/10.1193/1.2208088

Saatcioglu, M., Ghobarah, A., Nistor, I., 2006. Performance of Structures in Indonesia during the December 2004 Great Sumatra Earthquake and Indian Ocean Tsunami. Earthquake Spectra 22, 295–319. https://doi.org/10.1193/1.2209171

Schmidtlein, M.C., Wood, N.J., 2015. Sensitivity of tsunami evacuation modeling to direction and land cover assumptions. Applied Geography 56, 154–163. https://doi.org/10.1016/j.apgeog.2014.11.014

Shibayama, T., Esteban, M., Nistor, I., Takagi, H., Thao, N.D., Matsumaru, R., Mikami, T., Aranguiz, R., Jayaratne, R., Ohira, K., 2013. Classification of Tsunami and Evacuation Areas. Nat Hazards 67, 365–386. https://doi.org/10.1007/s11069-013-0567-4

Shrubsole, D., 2013. A history of flood management strategies in Canada revisited, in: Climate Change and Flood Risk Management. Edward Elgar Publishing, pp. 95–120. https://doi.org/10.4337/9781781006672.00009

Sun, Y., Yamori, K., Tanisawa, R., Kondo, S., 2013. Consciousness of Disaster Risk and Tsunami Evacuation: A Questionnaire Survey in Okitsu, Kochi Prefecture. Journal of Natural Disaster Science 34, 127–141. https://doi.org/10.2328/jnds.34.127

Suppasri, A., Shuto, N., Imamura, F., Koshimura, S., Mas, E., Yalciner, A.C., 2013. Lessons Learned from the 2011 Great East Japan Tsunami: Performance of Tsunami Countermeasures, Coastal Buildings, and Tsunami Evacuation in Japan. Pure Appl. Geophys. 170, 993–1018. https://doi.org/10.1007/s00024-012-0511-7

Swail, V.R., Cardone, V.J., Callahan, B., Ferguson, M., Gummer, D.J., Cox, A.T., 2007. THE MSC BEAUFORT WIND AND WAVE REANALYSIS, in: Proc. 10th Int. Workshop on Wave Hindcasting and Forecasting and Coastal Hazard Symp. WMO/IOC Joint Technical Commission for Oceanography and Marine Meteorology, North Shore, Oahu, Hawaii, p. 22.

Takabatake, T., Esteban, M., Nistor, I., Shibayama, T., Nishizaki, S., 2020a. Effectiveness of hard and soft tsunami countermeasures on loss of life under different population scenarios. International Journal of Disaster Risk Reduction 45, 101491. https://doi.org/10.1016/j.ijdrr.2020.101491

Takabatake, T., Fujisawa, K., Esteban, M., Shibayama, T., 2020b. Simulated effectiveness of a car evacuation from a tsunami. International Journal of Disaster Risk Reduction 47, 101532. https://doi.org/10.1016/j.ijdrr.2020.101532

Takabatake, T., Nistor, I., St-Germain, P., 2020c. Tsunami evacuation simulation for the District of Tofino, Vancouver Island, Canada. International Journal of Disaster Risk Reduction 48, 101573. https://doi.org/10.1016/j.ijdrr.2020.101573

Takabatake, T., Shibayama, T., Esteban, M., Achiari, H., Nurisman, N., Gelfi, M., Tarigan, T.A., Kencana, E.R., Fauzi, M.A.R., Panalaran, S., Harnantyari, A.S., Kyaw, T.O., 2019a. Field survey and evacuation behaviour during the 2018 Sunda Strait tsunami. Coastal Engineering Journal 61, 423–443. https://doi.org/10.1080/21664250.2019.1647963

Takabatake, T., St-Germain, P., Nistor, I., Stolle, J., Shibayama, T., 2019b. Numerical modelling of coastal inundation from Cascadia Subduction Zone tsunamis and implications for coastal communities on western Vancouver Island, Canada. Nat Hazards 98, 267–291. https://doi.org/10.1007/s11069-019-03614-3

Thomson, K., 1984. An Evaluation of Selected Canadian Flood Plain Management Policies (Doctoral Thesis). University of Toronto.

Topf, J., 2019. osmcode/osmcoastline [WWW Document]. GitHub. URL https://github.com/osmcode/osmcoastline (accessed 12.20.20).

United Nations Office for Disaster Risk Reduction, 2015. Sendai Framework for Disaster Risk Reduction 2015 - 2030.

Uno, K., Kashiyama, K., 2008. Development of simulation system for the disaster evacuation based on multi-agent model using GIS. Tinshhua Sci. Technol. 13, 348–353. https://doi.org/10.1016/S1007-0214(08)70173-1

US Indian Ocean Tsunami Warning System Program, 2007. How resilient is your coastal community? A guide for evaluating coastal community resilience to tsunamis and other hazards.

Völker, S., Kistemann, T., 2013. Reprint of: "I'm always entirely happy when I'm here!" Urban blue enhancing human health and well-being in Cologne and Düsseldorf, Germany. Social Science & Medicine 91, 141–152. https://doi.org/10.1016/j.socscimed.2013.04.016

Wang, H., Mostafizi, A., Cramer, L.A., Cox, D., Park, H., 2016. An agent-based model of a multimodal near-field tsunami evacuation: Decision-making and life safety. Transportation Research Part C: Emerging Technologies 64, 86–100. https://doi.org/10.1016/j.trc.2015.11.010

Watt, W.E., 1995. THE NATIONAL FLOOD DAMAGE REDUCTION PROGRAM: 1976 – 1995. Canadian Water Resources Journal 20, 237–247. https://doi.org/10.4296/cwrj2004237

Webster, T.L., Forbes, D.L., MacKinnon, E., Roberts, D., 2006. Flood-risk mapping for storm-surge events and sea-level rise using lidar for southeast New Brunswick. Canadian Journal of Remote Sensing 32, 194–211. https://doi.org/10.5589/m06-016

White, M.P., Alcock, I., Wheeler, B.W., Depledge, M.H., 2013. Coastal proximity, health and well-being: Results from a longitudinal panel survey. Health & Place 23, 97–103. https://doi.org/10.1016/j.healthplace.2013.05.006

Wood, N.J., Schmidtlein, M.C., 2013. Community variations in population exposure to near-field tsunami hazards as a function of pedestrian travel time to safety. Nat Hazards 65, 1603–1628. https://doi.org/10.1007/s11069-012-0434-8

World Meteorological Organization, 2011. Guide to storm surge forecasting. World Meteorological Organization, Geneva, Switzerland.

Xu, J., Murray, A., Wang, Z., Church, R., 2020. Challenges in applying capacitated covering models. Transactions in GIS 24, 268–290. https://doi.org/10.1111/tgis.12608

Yamakage, S., 2009. Modeling and expanding artificial societies: introduction to multi-agent simulation with artisoc.

Appendix

Table 5: The largest fifty positive surge events captured on Tuktoyaktuk Gauge 6485 that fall within the ERA5 time period. These were the surge events that simulated in the study conducted in Chapter 3.

ERA5 Event	Datetime	Measured Surge (m)
1	2019-07-21 9:00	1.49
2	2013-09-01 6:00	1.44
3	2017-11-04 9:00	1.42
4	2019-08-05 8:00	1.40
5	2018-08-17 16:00	1.34
6	2003-09-12 19:00	1.27
7	2018-09-01 13:00	1.25
8	2018-09-03 23:00	1.25
9	2013-10-30 12:00	1.23
10	2004-08-02 14:00	1.17
11	2013-11-12 7:00	1.17
12	2013-11-15 12:00	1.17
13	2015-08-27 21:00	1.12
14	2016-09-03 23:00	1.12
15	1991-08-24 7:00	1.11
16	2008-07-30 18:00	1.11
17	2004-08-14 13:00	1.08
18	2005-01-10 4:00	1.08
19	2019-08-12 8:00	1.07
20	2019-08-15 19:00	1.07
21	2010-11-19 3:00	1.05
22	2016-09-08 4:00	1.04
23	1982-08-21 15:00	1.03
24	2003-09-16 21:00	1.02
25	2008-10-08 0:00	1.00
26	1980-08-30 12:00	1.00
27	2017-07-25 19:00	0.99
28	2019-10-08 2:00	0.99
29	2018-07-05 18:00	0.99
30	2003-10-29 6:00	0.98
31	2019-08-24 7:00	0.97
32	2019-08-17 20:00	0.96
33	1980-09-16 9:00	0.96
34	2019-10-05 23:00	0.95
35	2003-10-05 9:00	0.94
36	2019-10-13 3:00	0.90
37	1991-08-09 6:00	0.90
38	1991-08-06 17:00	0.90
39	2019-11-02 11:00	0.90
40	2015-10-01 22:00	0.90
41	2019-10-31 8:00	0.88
42	2009-09-04 18:00	0.88
43	2009-09-07 7:00	0.88
44	2016-09-19 20:00	0.87
45	2016-09-24 11:00	0.86
46	2010-01-02 17:00	0.83
47	2018-07-31 22:00	0.82
48	2003-12-03 22:00	0.82
49	2006-07-03 8:00	0.82
50	2003-09-27 10:00	0.81